Non-Markovian decoherence theory for a double-dot charge qubit

Matisse W. Y. Tu and Wei-Min Zhang*
Department of Physics and Center for Quantum Information Science, National Cheng Kung University, Tainan 70101, Taiwan and National Center for Theoretical Science, Tainan 70101, Taiwan

(Received 20 September 2008; revised manuscript received 17 November 2008; published 19 December 2008)

In this paper, we develop a nonperturbation theory for describing decoherence dynamics of electron charges in a double quantum dot gated by electrodes. We extend the Feynman-Vernon influence functional theory to fermionic environments and derive an exact master equation for the reduced density matrix of electrons in the double dot for a general spectral density at arbitrary temperature and bias. We then investigate the decoherence dynamics of the double-dot charge qubit with backreaction of the reservoirs being fully taken into account. Time-dependent fluctuations and leakage effects induced from the dot-reservoir coupling are explicitly explored. The charge qubit dynamics from the Markovian to non-Markovian regime is systematically studied under various manipulating conditions. The decay behavior of charge qubit coherence and the corresponding relaxation time T_1 and dephasing time T_2 are analyzed in detail.

DOI: 10.1103/PhysRevB.78.235311 PACS number(s): 85.35.Be, 03.65.Yz, 03.65.Db, 03.67.Lx

I. INTRODUCTION

Double quantum dot systems have been attracting much attention because of their intriguing properties and their potential applications in nanotechnology and quantum information processing.[1,2] The basic structure of a double quantum dot system can be viewed as electrons confined in an electrostatic potential of double wells created by the fabricated gates, source, and drain electrodes in the heterostructure of a semiconductor. The heterostructure of GaAs/AlGaAs is a typical example of the realization of gate-defined double dot. The tunability of various couplings and energy levels in the dots makes it a promising quantum device (see, for example, Refs. 3–7). Moreover maintaining the electron coherence is important in making it part of a quantum information processor. However, fluctuations and dissipations brought up by quantum operations of manipulations and measurements as well as various features of the host material enrich the physics of double-dot systems more than perfect coherent evolution. Thus a lot of attention has been paid to investigate how various noises and interactions with the surroundings attenuate the coherent evolution of electrons in the double dot.

In this paper, we will concentrate on a nonperturbative dynamical theory for charge qubit manipulation with a double-dot system gated by electrodes. In the quantum computing scheme in terms of double dots where the electron charge degree of freedom is exploited, the effects in deviating the coherency of charge dynamics are summarized in the fluctuations of the interdot coupling and energy splitting between the two local charge states as well as the dissipation-induced damping effects. The amplitudes of these fluctuations can be estimated from measurements of the noise spectrum of electron currents and the minimum linewidth of elastic current peak.[1] Parallel theoretical works have been developed with different approaches in the literature for the purposes of both simulating the experimental results and understanding the physical mechanisms living in the double dot. In the present work, we shall extend the Feynman-Vernon influence functional theory[8] to fermionic environments and derive an exact master equation describing the coherent and decoherent dynamics of the electron charges in the double dot with the backreaction effects of the reservoirs being fully taken into account.

Stochastic noise processes resulted in a time-dependent Hamiltonian for the double dot have been widely analyzed in simulating the charge dynamics under noise influences. The Bloch-type rate equations for describing the double-dot transport properties was investigated by Gurvitz and Prager[9] using the many-body Schrödinger equation approach which is further applied to study decoherence of double-dot charge qubit in Ref. 10. The phonon-assisted processes was investigated within the Born-Markov regime by Brandes *et al.*[11] using Born-Markov typed master equation. A general expression of the qubit density matrix in case of pure dephasing[12] was used by Fedichkin and Fedorov[13] to study the error rate of the charge qubit. Stavrou and Hu[14] considered in detail the wave functions of the double-dot charge qubit for decoherence analysis. Karrasch *et al.*[15] came with the functional renormalization-group approach in dealing with the transport aspects of the multiple coupled dots. The non-Markovian dynamics was also recently studied by a suitable spin-boson model considering the acoustic phonons by Thorwart *et al.*[16,17] using numerical quasiadiabatic propagator path-integral scheme. Without Born-Markov approximation, Wu *et al.*[18,19] devised an analytical expression for the dynamical tunneling current using a perturbation treatment based on a unitary transformation. Effects from the Coulomb interaction between the dots and the gate electrodes with the formulation of kinetic equations was presented by Woodford *et al.*[20] The diversity in the methodologies and issues concerned in the literature shows the physical richness of this novel system.

As we can see there are many factors competing to play the consequent physics in the double quantum dot system. To single out one factor from the others on the resulted dynamical properties of this charge device, we shall first concentrate in this paper on the effects induced by dot-reservoir coupling, where the double dot is designed in the strong Coulomb blockade regime such that each dot only contains one energy level. The reservoirs consist of the source and drain electrodes which are controllable through the bias voltage. A schematic plot of the system is shown in Fig. 1. Thus the

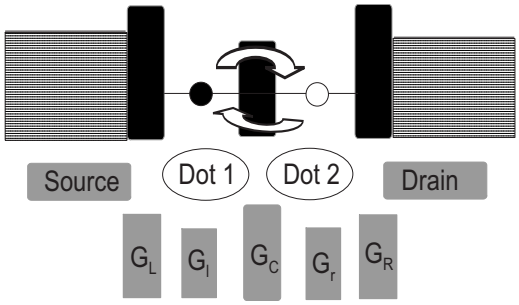

FIG. 1. A schematic plot for a lateral tunnel-coupled double quantum dot system.

total Hamiltonian of the system we concern in this work is given by

$$H = E_1 a_1^\dagger a_1 + E_2 a_2^\dagger a_2 + T_c(a_2^\dagger a_1 + a_1^\dagger a_2) + \sum_k (\varepsilon_{Lk} a_{Lk}^\dagger a_{Lk} + \varepsilon_{Rk} a_{Rk}^\dagger a_{Rk}) + \sum_k (t_{1Lk} a_1^\dagger a_{Lk} + t_{2Rk} a_{Rk}^\dagger a_2 + \text{H.c.}), \quad (1)$$

which contains the Hamiltonians of the double-dot, the source, and drain electrodes plus the interaction (electron tunneling processes) between them. The notations follow the convention and will be specified in detail later.

Our treatment is based on the exact master equation we derived for a general spectral density of the electron reservoirs at arbitrary temperature and bias:

$$\dot{\rho} = -i[H'(t), \rho] + \Gamma^0(t)\rho + \sum_{ij} \Gamma_{ij}(t)(2a_j \rho a_i^\dagger - a_i^\dagger a_j \rho - \rho a_i^\dagger a_j) + \sum_{ij} \Gamma_{ij}^\beta(t)(a_j \rho a_i^\dagger - a_i^\dagger \rho a_j - a_i^\dagger a_j \rho - \rho a_i^\dagger a_j), \quad (2)$$

where ρ is the reduced density matrix of the double dot obtained from the full density matrix of the double dot plus the reservoirs by tracing out the environmental degrees of freedom and

$$H'(t) = E_1'(t) a_1^\dagger a_1 + E_2'(t) a_2^\dagger a_2 + T_c'(t) a_1^\dagger a_2 + T_c'^*(t) a_2^\dagger a_1 \quad (3)$$

is the corresponding effective Hamiltonian. All the time-dependent coefficients in the above equations will be derived explicitly and nonperturbatively in Sec. III. The time-dependent fluctuations of the energy levels $E_i'(t)$ and the interdot transition amplitude $T_c'(t)$ are the renormalization effects risen from the electron tunneling processes between the double dot and the reservoirs. Other nonunitary terms describe the dissipative and noise processes with time-dependent coefficients, $\Gamma^0(t)$, $\Gamma(t)$, and $\Gamma^\beta(t)$, depicting the full non-Markovian decoherence dynamics. Equation (2) is obtained without considering the interdot Coulomb repulsion. But as we will show explicitly in Sec. III it is easy to extend to the strong interdot Coulomb repulsion regime where the strong interdot Coulomb repulsion simply leads one to exclude the states corresponding to a simultaneous occupation of two dots from Eq. (2). Then the exact master equation allows us to exploit the intrinsic quantum decoherence effects in the electron charge coherency brought up by the tunneling processes between the dots and the reservoirs through the bias controls.

Master equation (2) is derived by extending the Feynman-Vernon influence functional theory[8] to fermion coherent-state path integrals.[21] Historically, since it was first developed by Feynman and Vernon[8] in 1963 for quantum Brownian motion (QBM) modeled as a central harmonic oscillator linearly coupled to a set of harmonic oscillators simulating the thermal bath, the influence functional theory has been widely used to study dissipation dynamics in quantum tunneling problems[22] and decoherence problems in quantum measurement theory.[23,24] In these early applications, the master equation was derived for some particular class of ohmic environment.[25–27] The exact master equation for the QBM with a general spectral density at arbitrary temperature was obtained by Hu *et al.*[28] in 1992. Applications of the QBM exact master equation cover various topics, such as quantum decoherence, quantum-to-classical transition, and quantum measurement theory.[24] Very recently, such an exact master equation is further extended to the system of two entangled optical fields and two entangled harmonic oscillators for the study of non-Markovian entanglement dynamics in quantum information processing.[29,30] Nevertheless, using the influence functional theory to derive the exact master equation has been largely focused on the bosonic type of environments up to date.

On the other hand, the development of quantum transport theory in nanosystems has continuously attracted attention in the last two decades because of the great achievements in nanotechnology, where the reservoir is, in many cases, a fermion system. The traditional approach to study the quantum transport in nanosystems is the Schwinger-Keldysh nonequilibrium Green's-function formalism[31,32] which has been extensively used in successfully describing various quantum transport phenomena, such as Kondo effect, Fano resonance, and Coulomb blockade effects in quantum dots.[33–36] Master equations for quantum transport through quantum dots have also been derived but mostly in the perturbation theory up to the second order.[37–41] The exact master equation can be, in principle, obtained through the real-time diagrammatic expansion approach developed by Schon and co-workers,[35,42] as shown recently by Lee and Zhang.[43] Another interesting formalism is the recently published hierarchical expansion of the equations of motion for the reduced density matrix by Yan *et al.*[44] Nevertheless, in contrast to the bosonic environments,[28] an explicit formula of the exact master equation for fermionic environments with a general spectral density at arbitrary temperature and bias has not been carried out except for Eq. (2) in this work.

Unlike the quantum transport in nanosystems where people pay more attention on the tunneling current spectrum and its statistics, one cares in quantum information processing how the qubit coherency can be maintained for fast quantum operations where a strong coupling is required. Then a nonperturbative (with respect to the coupling between the system and its environment) master equation is more desirable for the precision manipulations of qubit states. Equation (2) obtained in this paper has fully taken into account the

backreaction of the electron reservoirs at arbitrary temperature and bias. This master equation is also valid for a general spectral density. It is a fully nonperturbative manner that goes far beyond the Born-Markov approximation often used in the literature. It enables us to explore the dynamics of the electron charge coherence in the double dot, from Markovian to non-Markovian regime under various manipulating conditions. Many other approximated master equations that have been developed in the literature can be obtained at well-defined limits of the present theory.

The rest of the paper is organized as follows. In Sec. II, we will use fermion coherent-state path-integral approach to solve exactly the electron dynamics in an isolated double quantum dots, as an illustration. We then extend the Feynman-Vernon influence functional theory originally built on the coordinate representation in quantum mechanics to fermion coherent-state representation. The exact master equation for the reduced density matrix of the double-dot system coupling to electron reservoirs is derived in Sec. III, where we also reproduce many other approximate master equations at well-defined limits of the present formulas. In Sec. IV, we investigate the non-Markovian decoherence dynamics of this device including the tunneling induced fluctuations in the energy splitting and interdot coupling of the double dot as well as the noise and dissipation effects on the charge mode populations and interferences. The leakage effect is also discussed together there. The decay behaviors of charge qubit coherence and the corresponding relaxation time T_1 and dephasing time T_2 are analyzed in detail. Extension of the present theory to other quantum dot systems is outlined in Sec. V and the conclusive remarks are given in Sec. VI. Appendixes A and B are presented for some detailed derivations.

II. FERMION COHERENT-STATE PATH-INTEGRAL APPROACH TO AN ISOLATED DOUBLE DOT

To illustrate the fermion coherent-state path-integral approach to the electron dynamics in a double quantum dot, we shall consider in this section a simple solvable system, a single electron in an isolated double dot, before we go to explore the realistic system in Sec. III. We also assume that each of the dots contains only one energy level, E_1 and E_2, respectively. The Hamiltonian of this isolated double quantum dot is

$$H = E_1 a_1^\dagger a_1 + E_2 a_2^\dagger a_2 + T_c(a_2^\dagger a_1 + a_1^\dagger a_2). \tag{4}$$

The notations follow the following convention: $a_{1,2}^\dagger$ are the creation operators for electrons in the double dot and T_c is the electron transition amplitude between the dots. In terms of the density operator, the time evolution of the system is described by

$$\rho(t) = U(t-t_0)\rho(t_0)U^\dagger(t-t_0), \tag{5}$$

where the density matrix $\rho(t)$ is the state of the system at a later time t, $\rho(t_0)$ is the state at the initial time t_0, $U(t-t_0) = \exp\{-\frac{i}{\hbar}H(t-t_0)\}$ is the evolution operator of the system, and we let $\hbar = 1$ hereafter.

Using the fermion coherent-state representation,[45] the density matrix at time t is expressed as $\langle\xi|\rho(t)|\eta\rangle = \rho(\xi^*, \eta, t)$, where ξ and η are the two Grassmann variables characterizing the two-mode fermion coherent states,

$$|\xi\rangle = \prod_{i=1,2} |\xi_i\rangle, \quad |\xi_i\rangle = \exp(-\xi_i a_i^\dagger)|0\rangle. \tag{6}$$

The fermion coherent state defined above is an eigenstate of the fermion annihilation operator, $a_i|\xi_i\rangle = \xi_i|\xi_i\rangle$. As these coherent states are overcomplete, they obey the resolution of identity, $\int d\mu(\xi)|\xi\rangle\langle\xi| = 1$, where the integration measure is defined by $d\mu(\xi) = \Pi_i e^{-\xi_i^*\xi_i} d\xi_i^* d\xi_i$. Note that the fermionic coherent states we used here are not normalized, and the normalization factors are moved into the above integration measure. Moreover, these coherent states are also nonorthogonal. The overlap of two fermionic coherent states is $\langle\xi|\xi'\rangle = \exp(\xi^\dagger\xi')$ with a matrix notation $\xi^\dagger = (\xi_1^* \xi_2^*)$.

The use of the coherent-state representation makes the path-integral formulation for a fermion system generally possible. In the fermionic coherent-state representation, the time evolution of the density matrix becomes

$$\rho(\xi_f^*, \eta_f, t) = \int d\mu(\xi_0) d\mu(\eta_0) \rho(\xi_0^*, \eta_0, t_0) \times J(\xi_f^*, \eta_f, t|\xi_0, \eta_0^*, t_0), \tag{7}$$

where $J(\xi_f^*, \eta_f, t|\xi_0, \eta_0^*, t_0) = \langle\xi_f|U(t-t_0)|\xi_0\rangle\langle\eta_0|U^\dagger(t-t_0)|\eta_f\rangle$ is the propagating function in which the forward and backward transition amplitudes $\langle\xi_f|U(t-t_0)|\xi_0\rangle$ and $\langle\eta_0|U^\dagger(t-t_0)|\eta_f\rangle$ can be solved exactly using path integral for Hamiltonian (4).

Explicitly, the fermion coherent-state path integral for the forward transition amplitude is given by

$$\langle\xi_f|U(t-t_0)|\xi_0\rangle = \int \mathcal{D}[\xi, \xi^*] \exp(iS_c[\xi^*, \xi]), \tag{8}$$

where the action is

$$S_c[\xi^*, \xi] = \sum_{i=1,2} \left\{ -\frac{i}{2}[\xi_{if}^* \xi_i(t) + \xi_i^*(t_0)\xi_{i0}] + \int_{t_0}^{t} d\tau \left[\frac{i}{2}(\xi_i^* \dot{\xi}_i - \dot{\xi}_i^* \xi_i) - (E_i \xi_i^* \xi_i + T_c \xi_i^* \xi_{i'}) \right] \right\}. \tag{9}$$

In the above equation, the path integral $\mathcal{D}[\xi, \xi^*]$ integrates over all paths $\xi_i(\tau)$ and $\xi_i^*(\tau)$ bounded by $\xi_i(t_0) = \xi_{i0}$ and $\xi_i^*(t) = \xi_{if}^*$, with $i \neq i'$. Since the action in Eq. (8) has a quadratic form, the path integral can be exactly carried out with the stationary path method.[45,46] The result is

$$\langle\xi_f|U(t-t_0)|\xi_0\rangle = \exp\sum_i \left[\frac{\xi_{if}^* \xi_i(t) + \xi_i^*(t_0)\xi_{i0}}{2} \right], \tag{10}$$

where $\xi_i^*(t_0)$ and $\xi_i(t)$ are determined by the solution of the equations of motion,

$$\dot{\xi}_i(\tau) + i[E_i \xi_i(\tau) + T_c \xi_{i'}(\tau)] = 0, \tag{11a}$$

$$\dot{\xi}_i^*(\tau) - i[E_i\xi_i^*(\tau) + T_c\xi_{i'}^*(\tau)] = 0, \tag{11b}$$

with the boundary conditions $\xi_i(t_0)=\xi_{i0}$ and $\xi_i^*(t)=\xi_{if}^*$, where $i\neq i'$. The backward transition amplitude $\langle\eta_0|U^\dagger(t-t_0)|\eta_f\rangle$ can be found by the same procedure. From Eq. (11) we can introduce a 2×2 matrix $u_0(t)$ such that $\xi(t)=u_0(t)\xi_0$ and $\xi^\dagger(t_0)=\xi_f^\dagger u_0(t)$, where $u_0(t)$ satisfies the equation of motion,

$$\dot{u}_0(t) + i\begin{pmatrix} E_1 & T_c \\ T_c & E_2 \end{pmatrix} u_0(t) = 0, \tag{12}$$

with the boundary condition $(u_0)_{ij}(t_0)=\delta_{ij}$. The solution of Eq. (12) is

$$\begin{aligned} u_0(t) &= \exp\left\{-i\begin{pmatrix} E_1 & T_c \\ T_c & E_2 \end{pmatrix}(t-t_0)\right\} \\ &= e^{-i\phi(t)}[\cos\,\varphi(t)I - i\mathbf{n}\cdot\boldsymbol{\sigma}\,\sin\,\varphi(t)], \end{aligned} \tag{13}$$

with $\phi(t)=E(t-t_0)$ and $\varphi(t)=\Omega_0(t-t_0)/2$. Here we have also defined $E\equiv\frac{1}{2}(E_1+E_2)$ and the Rabi frequency $\Omega_0=\sqrt{\varepsilon^2+\Delta^2}$, where $\varepsilon\equiv E_1-E_2$ is the energy-level splitting in the double dot and $\Delta=2T_c$ the interdot tunnel coupling. $\boldsymbol{\sigma}$ is the Pauli matrix, I is a 2×2 identity matrix, and the unit vector $\mathbf{n}\equiv(\Delta,0,\varepsilon)/\Omega_0$. Then the propagating function becomes

$$J(\xi_f^*,\eta_f,t|\xi_0,\eta_0^*,t_0) = \exp[\xi_f^\dagger u_0(t)\xi_0 + \eta_0^\dagger u_0^\dagger(t)\eta_f]. \tag{14}$$

If we use further the D algebra of fermion creation and annihilation operators in the fermion coherent-state representation $|\xi\rangle$,[21]

$$\xi_i|\xi\rangle = a_i|\xi\rangle, \quad -\frac{\partial}{\partial\xi_i}|\xi\rangle = a_i^\dagger|\xi\rangle, \tag{15a}$$

$$\langle\xi|\xi_i^* = \langle\xi|a_i^\dagger, \quad \langle\xi|\frac{\partial}{\partial\xi_i^*} = \langle\xi|a_i, \tag{15b}$$

it is easy to derive the equation of motion for the density operator $\rho(t)$:

$$\dot{\rho}(t) = \sum_{ij}\{[\dot{u}_0(t)u_0(t)^{-1}]_{ij}a_i^\dagger a_j\rho(t) + [\dot{u}_0(t)u_0(t)^{-1}]_{ij}^*\rho(t)a_j^\dagger a_i\}. \tag{16}$$

One can see from Eq. (12) that $\dot{u}_0(t)u_0(t)^{-1}=-i\left(\begin{smallmatrix} E_1 & T_c \\ T_c & E_2 \end{smallmatrix}\right)$. This simply reduces Eq. (16) to the familiar Liouvillian equation,

$$\dot{\rho}(t) = -i[H,\rho(t)], \tag{17}$$

as we expected. Having ensured the path-integral technique can reproduce the dynamical equation for an isolated double quantum dot, we will apply it to the double quantum dot coupling to electron reservoirs in Sec. III.

III. MASTER EQUATION FOR A DOUBLE QUANTUM DOT GATED BY ELECTRODES

A double quantum dot between two electron reservoirs, the source and drain electrodes controlled via a bias voltage (see Fig. 1), has a total Hamiltonian as

$$H = H_{\rm dot} + H_{\rm rev} + H_I, \tag{18}$$

where

$$H_{\rm dot} = E_1a_1^\dagger a_1 + E_2a_2^\dagger a_2 + T_c(a_2^\dagger a_1 + a_1^\dagger a_2) \tag{19a}$$

is the Hamiltonian of the double quantum dots,

$$H_{\rm rev} = \sum_k(\varepsilon_{Lk}a_{Lk}^\dagger a_{Lk} + \varepsilon_{Rk}a_{Rk}^\dagger a_{Rk}) \tag{19b}$$

is for the source and drain electrodes (reservoirs), and

$$H_I = \sum_k(t_{1Lk}a_1^\dagger a_{Lk} + t_{2Rk}a_{Rk}^\dagger a_2 + \text{H.c.}) \tag{19c}$$

is the coupling (interaction) between the double dot and the reservoirs that depicts the electron tunneling between them, where subscript k labels an electron state in the reservoirs, L and R denote the reservoirs of the source (left) and drain (right) electrodes, respectively, and $t_{1Lk}(t_{2Rk})$ is the electron tunneling amplitude between the source (drain) and the left (right) dot. Since we are only concerned in this work with the dynamics of charge qubit, we omitted spin degrees of freedom for electrons.

It should be pointed out that in Eq. (19a) we did not include explicitly the interdot Coulomb repulsion. This is because a typical interdot Coulomb energy is of the order of hundreds of μeV, which is much larger than the energy-level splitting ε and the interdot tunnel coupling Δ (both are of the order of tens of μeV or less) for charge qubit manipulation.[4] As a result, the interdot Coulomb interaction simply leads one to exclude the states corresponding to a simultaneous occupation of the two dots.[9,11] Thus, we will derive an exact master equation for the reduced density matrix of the double dot without considering the interdot Coulomb repulsion at beginning. The master equation of the double dot in the strong interdot Coulomb repulsion regime is then obtained from the exact master equation by explicitly excluding the states of doubly occupied two dots in terms of Bloch-type rate equations, as we will see later.

To derive nonperturbatively the master equation of the reduced density matrix for the double-dot system, we adopt the treatment of the Feynman-Vernon influence functional theory.[8] This approach within the framework of path-integral traces over the degrees of freedom of the environment (here the electrodes) into a functional of the dynamical variables of the system (the double quantum dot). This functional is called the influence functional by Feynman and Vernon,[8] which contains all the dynamical effects from the backreaction of the reservoirs to the system due to the coupling between them. Following the fermionic path-integral technique presented in Sec. II, we depict the route to an exact master equation aided with the results derived in detail in Appendixes A and B.

A. Influence functional

Explicitly, the total density matrix of the double dot plus the reservoirs obeys the quantum Liouvillian equation $i\partial\rho_{\rm tot}(t)/\partial t=[H,\rho_{\rm tot}(t)]$, which yields the formal solution

$$\rho_{\rm tot}(t) = e^{-iH(t-t_0)}\rho_{\rm tot}(t_0)e^{iH(t-t_0)}. \tag{20}$$

As we are interested in dynamics of the electrons in the double dot, we shall concentrate on the reduced density matrix for the double dot by tracing out the environmental variables, $\rho(t)=\mathrm{Tr}_E\,\rho_{\mathrm{tot}}(t)$. Assuming initially that the dots and the reservoirs are uncorrelated,[22,28] $\rho_{\mathrm{tot}}(t_0)=\rho(t_0)\otimes\rho_E(t_0)$, then the reduced density matrix describing the full dynamics of the electrons in the double dot becomes

$$\langle\xi_f|\rho(t)|\eta_f\rangle=\int d\mu(\xi_0)d\mu(\eta_0)\langle\xi_0|\rho(t_0)|\eta_0\rangle \times J(\xi_f^*,\eta_f,t|\xi_0,\eta_0^*,t_0), \tag{21}$$

where the propagating function is defined as

$$J(\xi_f^*,\eta_f,t|\xi_0,\eta_0^*,t_0)=\int \mathcal{D}[\xi^*\xi;\eta^*\eta]e^{i(S_c[\xi^*,\xi]-S_c^*[\eta^*,\eta])}\mathcal{F}[\xi^*\xi;\eta^*\eta], \tag{22}$$

with $S_c[\xi^*,\xi]$ being the action of the double dot in the fermion coherent-state representation given by Eq. (9) and $\mathcal{F}[\xi^*\xi;\eta^*\eta]$ is the influence functional which takes fully into account the backreaction effects of the reservoirs to the double dot and modifies the original action of the system into an effective one, $e^{(i/\hbar)(S_c[\xi^*,\xi]-S_c^*[\eta^*,\eta])}\mathcal{F}[\xi^*\xi;\eta^*\eta]=e^{(i/\hbar)S_{\mathrm{eff}}[\xi^*\xi;\eta^*\eta]}$. The path integral $\mathcal{D}[\xi^*\xi;\eta^*\eta]$ integrates over all paths $\xi^*(\tau)$, $\xi(\tau)$, $\eta^*(\tau)$, and $\eta(\tau)$ in the Grassmann space bounded by $\xi^*(t)=\xi_f^*$, $\xi(t_0)=\xi_0$, $\eta^*(t_0)=\eta_0^*$, and $\eta(t)=\eta_f$.

Let the reservoirs be initially in thermal equilibrium states at temperature β^{-1}; the influence functional can then be solved exactly with the result (see the derivation in Appendix A):

$$\mathcal{F}[\xi^*\xi;\eta^*\eta]=\exp\sum_{i=1,2}\left\{-\int_{t_0}^{t}d\tau\int_{t_0}^{\tau}d\tau'[F_{il}(\tau-\tau')\xi_i^*(\tau)\xi_i(\tau')+F_{il}^*(\tau-\tau')\eta_i^*(\tau')\eta_i(\tau)] -\int_{t_0}^{t}d\tau\int_{t_0}^{t}d\tau'[F_{il}(\tau-\tau')\eta_i^*(\tau)\xi_i(\tau')-F_{il}^{\beta}(\tau-\tau')(\eta_i^*(\tau)+\xi_i^*(\tau))(\eta_i(\tau')+\xi_i(\tau'))]\right\}. \tag{23}$$

The two time correlation functions in the influence functional,

$$F_{il}(\tau-\tau')=\sum_k|t_{ilk}|^2e^{-i\varepsilon_{lk}(\tau-\tau')}, \tag{24a}$$

$$F_{il}^{\beta}(\tau-\tau')=\sum_k f_l(\varepsilon_{lk})|t_{ilk}|^2e^{-i\varepsilon_{lk}(\tau-\tau')}, \tag{24b}$$

are called the dissipation-fluctuation kernels, where $f_l(\varepsilon_{lk})=\frac{1}{e^{\beta(\varepsilon_{lk}-\mu_l)}+1}$, with $l=L,R$ for $i=1,2$, respectively, are the Fermi distribution functions of the electron reservoirs, and $\mu_{L,R}$ are the corresponding chemical potentials. These nonlocal time-dependent functions contains the full dynamics effect from the reservoirs to the double dot. We should also point out that in the coherent-state representation, the influence functional for a many-fermion environment has a form similar to that of a many-boson environment[29] except for some sign difference due to the antisymmetric properties of fermion degrees of freedom.

The physical meaning of the above influence functional is very clear. The four terms contained in the exponential function of Eq. (23) correspond to four different physical processes in a time-closed path formalism (see Fig. 2). The first term gives the contribution of the backaction effect of the reservoirs to the double dot in terms of the time correlation function $F_{il}(\tau-\tau')$ of Eq. (24a) in the forward process from the time t_0 to the time t. For the double time integrals it contains, the first one starts from t_0 to τ and the second one from t_0 to t, sums over all the time sequences of the these propagations. Resummation of these propagating processes up to all orders of the system-reservoir coupling results in exactly the exponential function appearing in Eq. (23). Similar to the first term, the second term are just the backaction effect of the reservoirs to the system in the backward process from the time t back to the time t_0 which is just the complex conjugate of the first term. In terms of the Schwinger-Keldysh Green's-function approach, the time correlation function in these two propagating processes are just the time-ordered and antitime-ordered Green's functions. The histories of the forward paths $\xi_i^*(\tau),\xi_i(\tau)$ and the backward paths $\eta_i^*(\tau),\eta_i(\tau)$ are mixed up through the time correlation functions as shown in the third and the fourth terms in Eq. (23). The third term in Eq. (23) represents the mix of the forward and backward paths at time t. The last term is a mix of the forward and backward paths at time t_0 where the initial equilibrium properties of the reservoirs, i.e., the Fermi statistics and the temperature of the reservoirs, naturally enter into the time correlation function $F_{il}^{\beta}(\tau-\tau')$, as shown by Eq. (24b).

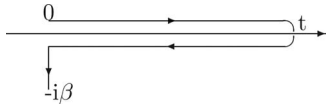

FIG. 2. The closed-time path for the trace of the density matrix of the reservoirs.

As we see all the influences of the reservoirs on the double dot are embedded in the two time-correlation functions, i.e., the two dissipation-fluctuation kernels [Eq. (24)] in the influence functional. These two dissipation-fluctuation kernels are related to each other through the dissipation-fluctuation theorem. This will become clear by introducing a spectral density defined as

$$J_{il}(\omega) = \sum_k |t_{ilk}|^2 \delta(\omega - \varepsilon_{lk}). \tag{25}$$

Obviously, the spectral density contains all the information about the reservoirs' density of states involved in the electron tunneling between the dots and reservoirs. Then time-correlation function (24) can be expressed as

$$F_{il}(\tau - \tau') = \int d\omega J_{il}(\omega) e^{-i\omega(\tau-\tau')}, \tag{26a}$$

$$F^{\beta}_{il}(\tau - \tau') = \int d\omega \frac{J_{il}(\omega) e^{-i\omega(\tau-\tau')}}{e^{\beta(\omega-\mu_l)} + 1}, \tag{26b}$$

This equation manifests the dissipation-fluctuation theorem in an open quantum system. It tells that all the backreaction effects of the reservoirs to the double dot are crucially determined by the spectral density $J_{il}(\omega)$.

B. Exact master equation

Now we can derive the master equation for the reduced density matrix. As we see the effective action after integrating out the environmental degrees of freedom, i.e., combining Eqs. (22) and (23) together, still has a quadratic form in terms of the dynamical variables of the fermion coherent states. Thus the path integral [Eq. (22)] can be solved exactly by utilizing the stationary path method and Gaussian integrals.[45,46] The resulting propagating function is simply given by

$$J(\xi^*_f, \eta_f, t|\xi_0, \eta^*_0, t_0) = A(t) \exp \sum_{i=1,2} \left[\frac{\xi^*_{if}\xi_i(t) + \xi^*_i(t_0)\xi_{i0}}{2} + \frac{\eta^*_{i0}\eta_i(t_0) + \eta^*_i(t)\eta_{if}}{2} \right], \tag{27}$$

where $A(t)$ is the contribution arisen from the fluctuations around the stationary paths which will be given later. The stationary paths $\xi_i(t)$ and $\eta_i(t_0)$ are determined by the equations of motion,

$$\dot{\xi}_i(\tau) + i[E_i\xi_i(\tau) + T_c\xi_{i'}(\tau)] + \int_{t_0}^{\tau} d\tau' F_{il}(\tau - \tau')\xi_i(\tau') - \int_{t_0}^{t} d\tau' F^{\beta}_{il}(\tau - \tau')[\xi_i(\tau') + \eta_i(\tau')] = 0, \tag{28a}$$

$$\dot{\eta}_i(\tau) + i[E_i\eta_i(\tau) + T_c\eta_{i'}(\tau)] + \int_{t_0}^{\tau} d\tau' F_{il}(\tau - \tau')\eta_i(\tau') - \int_{t_0}^{t} d\tau' F_{il}(\tau - \tau')[\eta_i(\tau') + \xi_i(\tau')] + \int_{t_0}^{t} d\tau' F^{\beta}_{il}(\tau - \tau')[\eta_i(\tau') + \xi_i(\tau')] = 0, \tag{28b}$$

subjected to the boundary condition $\xi_i(t_0) = \xi_{i0}$ and $\eta_i(t) = \eta_{if}$, while $\xi^*_i(t_0)$ and $\eta^*_i(t)$ in Eq. (27) can be obtained from the complex conjugate equations of Eqs. (28a) and (28b), respectively, under the boundary condition $\xi^*_i(t) = \xi^*_{if}$ and $\eta^*_i(t_0) = \eta^*_{i0}$. The local terms $\dot{\xi}_i + i(E_i\xi_i + T_c\xi_{i'})$ and $\dot{\eta}_i + i(E_i\eta_i + T_c\eta_{i'})$ in Eq. (28) are intrinsic and well describe the coherent dynamics of the electron states in an isolated double quantum dot, as we have discussed in Sec. II. The nonlocal terms involving two different time correlation functions, $F_{il}(\tau - \tau')$ and $F^{\beta}_{il}(\tau - \tau')$, stem from the coupling to the reservoirs. These two time correlation functions play quite distinct roles in the equations of motion. The interaction between the double dot and the electron reservoirs is mediated through electron tunnelings between them. The correlation $F_{il}(\tau - \tau')$ describes the backaction of the reservoirs to the double dot due to the interaction between them. However, the correlation function $F^{\beta}_{il}(\tau - \tau')$ also harbors the Fermi-Dirac statistic effect of the electron reservoirs which exists even in the zero-temperature limit. The latter situation is quite different from a bosonic environment where $F^{\beta}_{il}(\tau - \tau')$ vanishes at zero temperature.[29]

The solutions of $\xi_i(t)$, $\eta_i(t_0)$ and $\eta^*_i(t)$, $\xi^*_i(t_0)$ determined by Eq. (28) and its complex conjugate can be factorized from the corresponding boundary conditions. It is not too difficult to find that

$$\xi(t) = [I - v(t)]^{-1}[u(t)\xi_0 + v(t)\eta_f], \tag{29a}$$

$$\eta(t_0) = u^{\dagger}(t)\{I + [I - v(t)]^{-1}v(t)\}\eta_f - \{I - u^{\dagger}(t)[I - v(t)]^{-1}u(t)\}\xi_0. \tag{29b}$$

Here we have again used the matrix notation $\xi^T = (\xi_1 \xi_2)$ and a same form for η. The new dynamical variables expressed as two time-dependent 2×2 matrices, $u(\tau)$ and $v(\tau)$, satisfy the dissipation-fluctuation integrodifferential equations:

$$\dot{u}(\tau) + iMu(\tau) + \int_{t_0}^{\tau} d\tau' G(\tau - \tau')u(\tau') = 0, \tag{30a}$$

$$\dot{v}(\tau) + iMv(\tau) + \int_{t_0}^{\tau} d\tau' G(\tau - \tau')v(\tau') = \int_{t_0}^{t} d\tau' G^{\beta}(\tau - \tau')\bar{u}(\tau'), \tag{30b}$$

with the boundary conditions $u_{ij}(t_0) = \delta_{ij}$ and $v_{ij}(t_0) = 0$, while $\bar{u}(\tau)$ in Eq. (30b) obeys the backward equation of motion to $u(\tau)$, namely, $\bar{u}(\tau) = u^{\dagger}(t + t_0 - \tau)$ for $t_0 \le \tau \le t$. In Eq. (30), we have also defined the 2×2 matrices $M = \begin{pmatrix} E_1 & T_c \\ T_c & E_2 \end{pmatrix}$, $G_{ij}(\tau - \tau')$

$=F_{il}(\tau-\tau')\delta_{ij}$, and $G^{\beta}_{ij}(\tau-\tau')=F^{\beta}_{il}(\tau-\tau')\delta_{ij}$. As we see $u(\tau)$ is determined purely by $F_{il}(\tau-\tau')$ while $v(\tau)$ depends on both correlation functions $F_{il}(\tau-\tau')$ and $F^{\beta}_{il}(\tau-\tau')$. The full complexity of the non-Markovian dynamics of charge coherence in the double dot induced from its coupling to the reservoirs is thus manifested through these equations of motion.

As $\xi^*_i(t_0)$ and $\eta^*_i(t)$ satisfy, respectively, the complex conjugate equations of $\eta_i(\tau)$ and $\xi_i(\tau)$ with the boundary condition $\xi^*_i(t)=\xi^*_{if}$ and $\eta^*_i(t_0)=\eta^*_{i0}$, it is easy to find the similar solution from Eq. (29) for $\xi^*_i(t_0)$ and $\eta^*_i(t)$. Substituting these results into Eq. (27) and note the fact that $v(\tau)$ is a Hermitian matrix at $\tau=t$, we obtain explicitly the exact propagating function of the double-dot system:

$$J(\xi^*_f,\eta_f,t|\xi_0,\eta^*_0,t_0)=A(t)\exp\{\xi^\dagger_f J_1(t)\xi_0+\xi^\dagger_f J_2(t)\eta_f+\eta^\dagger_0 J_3(t)\xi_0+\eta^\dagger_0 J^\dagger_1(t)\eta_f\}, \tag{31}$$

where

$$J_1(t)=w(t)u(t),\quad J_2(t)=w(t)-I, \tag{32a}$$

$$J_3(t)=u^\dagger(t)w(t)u(t)-I,\quad A(t)=1/\det[w(t)], \tag{32b}$$

with $w(t)=[I-v(t)]^{-1}$. All these time-dependent coefficients can be fully determined by solving Eq. (30).

Once the exact propagating function is obtained, the dynamics of the reduced density matrix [Eq. (21)], which fully takes into account the backreaction of the electron reservoirs, can be completely solved for any given initial electron state of the double dot. The explicit solution of the reduced density matrix relies solely on the solution to the equations of motion [Eq. (30)] which, in general, has to be solved numerically. To check the consistency, we may let the double dot be decoupled from the electron reservoirs, namely, set $t_{ilk}=0$, then the dissipation-fluctuation kernels vanish. As a result, Eq. (30a) is reduced to Eq. (12) and $u(t)$ is reduced to $u_0(t)$ whose solution is given after Eq. (12), while the solution of Eq. (30b) gives $v(t)=0$. Consequently the propagating function Eq. (31) is reduced to Eq. (14) which recovers the exact solution of the isolated double-dot system shown in Sec. II.

Having the explicit form of propagating function (31) in hand, it is straightforward to derive the master equation for the reduced density matrix directly from Eq. (21). Here we shall deduce an operator form of the master equation such that all the time-dependent coefficients in the master equation are explicitly independent of the initial state of the double dot as well as of any specific representation. Taking the time derivative to Eq. (31), eliminating the initial state dependence and using the D-algebra of the fermion creation and annihilation operators in the fermion coherent-state representation [Eq. (15)], the exact master equation of the double dot with a general spectral density at arbitrary temperature and bias is given by

$$\begin{aligned}\dot\rho(t)=&\sum_{ij}\{\Omega_{ij}(t)[a^\dagger_i a_j,\rho(t)]\\&+\Gamma_{ij}(t)[2a_j\rho(t)a^\dagger_i-a^\dagger_i a_j\rho(t)-\rho(t)a^\dagger_i a_j]\\&+\Gamma^{\beta}_{ij}(t)[a_j\rho(t)a^\dagger_i-a^\dagger_i\rho(t)a_j-a^\dagger_i a_j\rho(t)-\rho(t)a^\dagger_i a_j]\}\\&+\Gamma^0(t)\rho(t),\end{aligned} \tag{33}$$

where all time-dependent coefficients in Eq. (33) are determined by $u(t)$ and $v(t)$ through the following relations:

$$\Omega_{ij}(t)=\frac{1}{2}[\dot u u^{-1}-(u^\dagger)^{-1}\dot u^\dagger]_{ij}, \tag{34a}$$

$$\Gamma_{ij}(t)=-\frac{1}{2}[\dot u u^{-1}+(u^\dagger)^{-1}\dot u^\dagger]_{ij}, \tag{34b}$$

$$\Gamma^{\beta}_{ij}(t)=[\dot u u^{-1}v+v(u^\dagger)^{-1}\dot u^\dagger-\dot v]_{ij}, \tag{34c}$$

and $\Gamma^0(t)=\mathrm{Tr}\,\Gamma^{\beta}$. The first term in the master equation is indeed the generalized Liouvillian term which can be explicitly written as

$$\sum_{ij}\Omega_{ij}(t)[a^\dagger_i a_j,\rho(t)]=-i[H'(t),\rho(t)], \tag{35a}$$

where

$$H'(t)=E'_1(t)a^\dagger_1 a_1+E'_2(t)a^\dagger_2 a_2+T'_c(t)a^\dagger_1 a_2+T'^*_c(t)a^\dagger_2 a_1 \tag{35b}$$

is an effective Hamiltonian of the double quantum dot with the shifted (renormalized) time-dependent energy levels and the shifted interdot transition amplitude,

$$E'_i(t)=i\Omega_{ii}\quad(i=1,2),\quad T'_c(t)=i\Omega_{12}. \tag{36a}$$

Using the equation of motion [Eq. (30a)], we further obtain

$$E'_i(t)=E_i-\mathrm{Im}[W_{ii}(t)],\quad i=1,2, \tag{36b}$$

$$T'_c(t)=T_c+\frac{i}{2}[W_{12}(t)-W^*_{21}(t)], \tag{36c}$$

where

$$W(t)=\int_{t_0}^{t}d\tau\begin{pmatrix}F_{1L}(t-\tau) & 0\\ 0 & F_{2R}(t-\tau)\end{pmatrix}u(\tau)u(t)^{-1}. \tag{36d}$$

Combining Eqs. (33) and (34) together lead to master equation (2) presented in Sec. I. It shows that the shifted energy levels, $E'_{1,2}(t)$, and the interdot transition amplitude, $T'_c(t)$, are entirely contributed by $u(t)$ that involves only the time correlation function $F_{il}(t-\tau)$. The rest of Eq. (33) describes the dissipation and noise processes of electron charges with non-Markovian behaviors having been embedded in these time-dependent 2×2 matrix coefficients, $\Gamma(t)$ and $\Gamma^{\beta}(t)$. We call $\Gamma(t)$ and $\Gamma^{\beta}(t)$ the dissipation-fluctuation matrix coefficients or simply the dissipation-fluctuation coefficients hereafter. Note that $\Gamma(t)$ is solely determined by $u(t)$, and $\Gamma^{\beta}(t)$ is given by both $u(t)$ and $v(t)$ where the temperature dependence is explicitly described by $v(t)$ through the temperature-dependent time correlation function $F^{\beta}_{il}(t-\tau)$. Thus all the time-dependent coefficients in the master equation are nonperturbatively determined by dissipation-fluctuation equation of motion (30) and fully account for the backreaction effects of the reservoirs to the double dot.

C. Relating to the perturbative/Markov master equations

Currently, master equations for open quantum systems are mostly obtained based on perturbation and/or Markov approximations; it is certainly interesting to show how the perturbative or Markov master equations for this double-dot system can be reduced from the above exact non-Markovian master equation. As we have pointed out the full non-Markovian dynamics is depicted by the time-dependent coefficients in the exact master equation, $E_i'(t)$, $T_c'(t)$, $\Gamma(t)$, and $\Gamma^\beta(t)$, and these coefficients are completely determined by dissipation-fluctuation equation of motion (30). The perturbative or Markov master equations can be simply gotten by either taking a perturbative expansion in terms of coupling strength or ignoring the backreaction memory effect from the environment.

1. Perturbative expansion

The perturbative expansion can be applied to the equation of motion [Eq. (30a)] straightforwardly. Let

$$u(\tau) = u_0(\tau) + u_2(\tau) + u_4(\tau) + \cdots, \tag{37}$$

where $u_{2n}(\tau)$, $n=0,1,2,\ldots$, is the $2n$th order contribution in terms of the coupling strength t_{ilk} [corresponding to the nth order in terms of the time correlation functions $F_{il}(\tau-\tau')$, the matrix elements of $G(\tau-\tau')$ in Eq. (30)]. The solution to the zero order, $u_0(\tau)$, is already given by Eq. (13) in Sec. II, i.e., $u_0(\tau)=\exp\{-iM(\tau-t_0)\}$. It is easy to find

$$u_2(\tau) = -u_0(\tau)\int_{t_0}^{\tau} d\tau' u_0^{-1}(\tau')\int_{t_0}^{\tau'} d\tau'' G(\tau'-\tau'')u_0(\tau''), \tag{38a}$$

$$u_4(\tau) = -u_0(\tau)\int_{t_0}^{\tau} d\tau' u_0^{-1}(\tau')\int_{t_0}^{\tau'} d\tau'' G(\tau'-\tau'')u_2(\tau''), \tag{38b}$$

The nonexistence of odd powers of the coupling strength in the above expansion is due to the backaction between the system and environment, namely, the contribution comes from electrons tunnel from the environment into the dots and then tunnel back to the environment. The solution to Eq. (30b) is also easy to obtain,

$$v(\tau) = v_0(\tau) + v_2(\tau) + \cdots = 0 + u_0(\tau)\int_{t_0}^{\tau} d\tau' u_0^{-1}(\tau')\int_{t_0}^{t} d\tau'' G^\beta(\tau'-\tau'')\bar{u}_0(\tau'') + \cdots. \tag{39}$$

It is indeed not difficult to find the solution of Eq. (30) to all orders in this perturbative expansion.

Substituting the above solutions into the time-dependent coefficients, we can systematically resolve the perturbative expansion of the non-Markovian master equation order by order in terms of the coupling strength. If the coupling strength is much smaller in comparison with the interdot coupling T_c in the double dot, one can take the expansion only up to the second order of the coupling strength. Then,

$$\dot{u}(t)u(t)^{-1} \approx -iM - \int_{t_0}^{t} d\tau G(t-\tau)u_0(\tau)u_0^{-1}(t), \tag{40a}$$

$$\dot{u}(t)u(t)^{-1}v(t) + v(t)[u^\dagger(t)]^{-1}\dot{u}^\dagger(t) - \dot{v}(t) \approx -\int_{t_0}^{t} d\tau G^\beta(t-\tau)\bar{u}_0(\tau) + \text{H.c.} \tag{40b}$$

All the coefficients in the master equation, $E_i'(t)$, $T_c'(t)$, $\Gamma(t)$, and $\Gamma^\beta(t)$, can be explicitly calculated using relationships (34) and (36). The resulting master equation is the second-order master equation in the perturbation theory.

2. Markov approximation

It is also interesting to see how the conventional Markov dynamics can be directly obtained from our exact non-Markovian master equation under Markov approximation. Markov approximation is given by $u_{ij}(\tau')e^{iE_i(\tau'-t_0)} \cong u_{ij}(\tau)e^{iE_i(\tau-t_0)}$ and $v_{ij}(\tau')e^{iE_i(\tau'-t_0)} \cong v_{ij}(\tau)e^{iE_i(\tau-t_0)}$, namely, approximately taking the dynamical variables $u(\tau), v(\tau)$ to the ones that depend only on the present time so that any memory regarding the earlier time can be ignored. Such a Markov approximation is mainly based on the physical assumption that the correlation time (memory time) of environment is very small compared with the typical time scale of the system evolution. Also under this assumption we can take the time limit $(t-t_0, \tau-t_0 \to \infty)$,[47] and then the integral kernels in Eq. (30) reduce to

$$\int_{t_0}^{\tau} d\tau' F_{il}(\tau-\tau')u_{ij}(\tau') \approx \left(\frac{\Gamma_l}{2} + i\delta E_i\right)u_{ij}(\tau), \tag{41a}$$

$$\int_{t_0}^{t} d\tau' F_{il}^\beta(\tau-\tau')\bar{u}_{ij}(\tau') \approx f_l\Gamma_l\bar{u}_{ij}(\tau), \tag{41b}$$

where $\delta E_i = \mathcal{P}\int_0^\infty \frac{J_{il}(\omega)d\omega}{\omega-E_i}$ ($\mathcal{P}$ denotes the Cauchy principal value) and $\Gamma_l = 2\pi J_{il}(E_i)$ is the contribution from the integration pole with $l=L,R$ for $i=1,2$, respectively. $f_{L,R}$ are the Fermi distribution functions of the reservoirs. In this Markov approximation, the equation of motion [Eq. (30)] can be solved analytically and the solution is

$$u(t) = \exp\left\{-\begin{pmatrix} iE_1' + \frac{\Gamma_L}{2} & iT_c \\ iT_c & iE_2' + \frac{\Gamma_R}{2} \end{pmatrix}(t-t_0)\right\}, \tag{42a}$$

$$v(t) = \int_{t_0}^{t} d\tau u(t+t_0-\tau)\begin{pmatrix} f_L\Gamma_L & 0 \\ 0 & f_R\Gamma_R \end{pmatrix}\bar{u}(\tau), \tag{42b}$$

where $E_i' = E_i + \delta E_i$.

With the above explicit solution for $u(t)$ and $v(t)$, we can calculate all the coefficients in the master equation in the Markov approximation. Noting that $\bar{u}(\tau) = u^\dagger(t+t_0-\tau)$, it is easy to find

$$\dot{u}u^{-1} = -\begin{pmatrix} iE_1' + \frac{\Gamma_L}{2} & iT_c \\ iT_c & iE_2' + \frac{\Gamma_R}{2} \end{pmatrix}, \tag{43a}$$

$$\dot{u}u^{-1}v + v(u^{\dagger})^{-1}\dot{u}^{\dagger} - \dot{v} = -\begin{pmatrix} f_L\Gamma_L & 0 \\ 0 & f_R\Gamma_R \end{pmatrix}. \tag{43b}$$

As a result, in the Markov approximation, all the time-dependent coefficients in the master equation become constants:

$$E_{1,2}'(t) = E_{1,2} + \delta E_{1,2}, \quad T_c'(t) = T_c, \tag{44a}$$

$$\Gamma_{ij}(t) = \frac{1}{2}\Gamma_l\delta_{ij}, \quad \Gamma_{ij}^{\beta}(t) = -f_l\Gamma_l\delta_{ij}. \tag{44b}$$

Non-Markovian master equation (33) is then reduced to the Markov master equation. It is worth pointing out that this Markov approximation is valid to all kinds of spectral densities. A different spectral density may produce the energy-level shift, $\delta E_i = \mathcal{P}\int \frac{J_{il}(\omega)d\omega}{\omega - E_i}$, and decay rate, $\Gamma_l = 2\pi J_{il}(E_i)$, differently. As a result, our exact non-Markovian master equation can explore not only more complicated situation where Markov approximation is unreachable but also different spectral densities between the system and the environment even in the Markovian limit.

Furthermore, it is easy to check that Eq. (44) can also be obtained by applying Markov approximation (41) into second-order perturbation solution (40). In other words, the Markov approximation only accounts the second-order contribution from the system-environment coupling. This is because neglecting the environmental memory effect automatically ignores the backreaction effects of the environment to the system. The backreaction here is defined as electrons correlatively tunnel forth and back between the environment and the dots for many times, which corresponds to high-order contributions in the perturbation expansion. For a weak-coupling strength, the second-order perturbative master equation could be a good approximation where non-Markovian decoherence is partially taken into account. If the environmental time scale is much shorter than the typical time scale of the double dot, the Markov master equation can also give a good description to the decoherence dynamics. However, for the double-dot charge qubit gated by electrodes, the coupling strength between the dots and electrodes is comparable to the interdot coupling of the double dot, and the environmental time scale of the electrodes is also of the same order of the Rabi frequency of the charge qubit.[4] Then, a fully nonperturbative and non-Markovian master equation will become useful for understanding decoherence dynamics of the charge qubit.

D. Bloch-type rate equations for zero and strong interdot Coulomb repulsion cases

1. No interdot Coulomb repulsion

To closely examine the decoherence of electron charge dynamics in the double dot, it is more convenient to rewrite master equation (33) as a set of Bloch-type rate equations in terms of the localized charge states in the double dot. Without considering the interdot Coulomb repulsion, the rate equations can be obtained directly from master equation (33) in the charge configuration space containing the states of empty double dot, the first dot occupied, the second dot occupied, and both dots occupied. We label these four states by $|j\rangle, j=0,1,2,3$. Then the master equation in the above basis becomes

$$\dot{\rho}_{00} = \tilde{\Gamma}_{11}\rho_{11} + \tilde{\Gamma}_{21}\rho_{12} + \tilde{\Gamma}_{12}\rho_{21} + \tilde{\Gamma}_{22}\rho_{22} + \Gamma^0\rho_{00}, \tag{45a}$$

$$\dot{\rho}_{11} = (\Gamma^0 - 2\bar{\Gamma}_{11})\rho_{11} + \bar{\Xi}_{-}^{*}\rho_{12} + \bar{\Xi}_{-}\rho_{21} - \Gamma_{11}^{\beta}\rho_{00} + \tilde{\Gamma}_{22}\rho_{33}, \tag{45b}$$

$$\dot{\rho}_{22} = (\Gamma^0 - 2\bar{\Gamma}_{22})\rho_{22} + \bar{\Xi}_{+}^{*}\rho_{12} + \bar{\Xi}_{+}\rho_{21} - \Gamma_{22}^{\beta}\rho_{00} + \tilde{\Gamma}_{11}\rho_{33}, \tag{45c}$$

$$\dot{\rho}_{12} = [-i\varepsilon' + \Gamma^0 - \mathrm{Tr}\,\bar{\Gamma}]\rho_{12} + \bar{\Xi}_{+}\rho_{11} + \bar{\Xi}_{-}\rho_{22} - \Gamma_{12}^{\beta}\rho_{00} + \tilde{\Gamma}_{12}\rho_{33}, \tag{45d}$$

$$\dot{\rho}_{33} = \Gamma_{12}^{\beta}\rho_{21} + \Gamma_{21}^{\beta}\rho_{12} - \Gamma_{11}^{\beta}\rho_{22} - \Gamma_{22}^{\beta}\rho_{11} + (\Gamma^0 - 2\mathrm{Tr}\bar{\Gamma})\rho_{33}. \tag{45e}$$

Here the density-matrix elements are defined by $\rho_{ij} = \langle i|\rho|j\rangle$. We have also defined all the time-dependent coefficients in the rate equations as $\tilde{\Gamma}(t) = 2\Gamma(t) + \Gamma^{\beta}(t)$, $\bar{\Gamma}(t) = \Gamma(t) + \Gamma^{\beta}(t)$, $\bar{\Xi}_{\pm} = \pm iT_c'(t) - \bar{\Gamma}_{12}$, and $\varepsilon'(t) = E_1'(t) - E_2'(t)$, where $E_i'(t)$, $T_c'(t)$, $\Gamma(t)$, $\Gamma^{\beta}(t)$, and $\Gamma^0(t)$ are the time-dependent transport coefficients contained in the master equation and are explicitly given by Eqs. (34) and (36). These time-dependent coefficients in the rate equations thus fully characterize the non-Markovian dynamics of electrons in the double dot. The first and the last rate equations account for electron charge leakage effects in this device, while other three rate equations depict charge qubit decoherence dynamics under the influence of the reservoirs.

For a constant spectral density that has been widely used in the literature, the time-correlation function becomes

$$F_{il}(\tau - \tau') \to \frac{\Gamma_l}{2\pi}\int_{-\infty}^{\infty} d\omega e^{-i\omega(\tau-\tau')} = \Gamma_l\delta(\tau - \tau'), \tag{46}$$

where $\Gamma_l = 2\pi\rho_l|t_{ilk}|^2$ ($l = L,R$ for $i = 1,2$) and $\rho_{L,R}$ are the densities of states for the left and right electron reservoirs. Then in the Markovian limit ($t - t_0, \tau - t_0 \to \infty$),[47] the integral kernels in Eq. (30) reduce to

$$\int_{t_0}^{\tau} d\tau' F_{il}(\tau - \tau')u_{ij}(\tau') \approx \frac{1}{2}\Gamma_l u_{ij}(\tau), \tag{47a}$$

$$\int_{t_0}^{t} d\tau' F_{il}^{\beta}(\tau - \tau')\bar{u}_{ij}(\tau') \approx f_l\Gamma_l\bar{u}_{ij}(\tau). \tag{47b}$$

The factor $\frac{1}{2}$ in Eq. (47a) comes from the boundary of the time integration sitting upon τ, and $f_{L,R}$ in Eq. (47b) are the

Fermi distribution functions of the reservoirs.

Comparing Eq. (47) with Eq. (41), it shows that a constant spectral density naturally leads to the Markov approximation with $\delta E_i=0$. As a result, for a constant spectral density in the Markovian limit, all the time-dependent coefficients in the master equation become constant:

$$E'_{1,2}(t) \approx E_{1,2}, \quad T'_c(t) \approx T_c, \tag{48a}$$

$$\Gamma_{ij}(t) \approx \frac{1}{2}\Gamma_l \delta_{ij}, \quad \Gamma^{\beta}_{ij}(t) \approx -f_l \Gamma_l \delta_{ij}. \tag{48b}$$

In other words, in the Markovian limit with a constant spectral density, there is no renormalization effect to the energy-level shift and the interdot transition amplitude. The dissipation-fluctuation effects are simply reduced to the time-independent tunneling rates between the dots and the reservoirs. In fact, the differences of time-dependent and time-independent coefficients manifest the non-Markovian dynamics of electron charges in the double dot. We shall present quantitatively such differences in Sec. IV.

For a constant spectral density in the Markovian limit, the rate equations are simply reduced to

$$\dot{\rho}_{00} = \bar{f}_L \Gamma_L \rho_{11} + \bar{f}_R \Gamma_R \rho_{22} - (f_L \Gamma_L + f_R \Gamma_R)\rho_{00}, \tag{49a}$$

$$\dot{\rho}_{11} = -(\bar{f}_L \Gamma_L + f_R \Gamma_R)\rho_{11} + iT_c(\rho_{12} - \rho_{21}) + f_L \Gamma_L \rho_{00} + \bar{f}_R \Gamma_R \rho_{33}, \tag{49b}$$

$$\dot{\rho}_{22} = -(\bar{f}_R \Gamma_R + f_L \Gamma_L)\rho_{22} - iT_c(\rho_{12} - \rho_{21}) + f_R \Gamma_R \rho_{00} + \bar{f}_L \Gamma_L \rho_{33}, \tag{49c}$$

$$\dot{\rho}_{12} = \left(-i\varepsilon - \frac{\Gamma_L + \Gamma_R}{2}\right)\rho_{12} + iT_c(\rho_{11} - \rho_{22}), \tag{49d}$$

$$\dot{\rho}_{33} = -(\bar{f}_L \Gamma_L + \bar{f}_R \Gamma_R)\rho_{33} + f_L \Gamma_L \rho_{22} + f_R \Gamma_R \rho_{11}, \tag{49e}$$

where $\bar{f}_{L,R}=(1-f_{L,R})$ and $\varepsilon=E_1-E_2$. Under the large bias limit, $f_L=1$, $f_R=0$, the above rate equations reproduce the rate equations obtained by Gurvitz and Prager[9] for the double dot without considering the interdot Coulomb repulsion:

$$\dot{\rho}_{00} = -\Gamma_L \rho_{00} + \Gamma_R \rho_{22}, \tag{50a}$$

$$\dot{\rho}_{11} = \Gamma_L \rho_{00} + \Gamma_R \rho_{33} + iT_c(\rho_{12} - \rho_{21}), \tag{50b}$$

$$\dot{\rho}_{22} = -(\Gamma_L + \Gamma_R)\rho_{22} - iT_c(\rho_{12} - \rho_{21}), \tag{50c}$$

$$\dot{\rho}_{12} = \left(-i\varepsilon - \frac{\Gamma_L + \Gamma_R}{2}\right)\rho_{12} + iT_c(\rho_{11} - \rho_{22}), \tag{50d}$$

$$\dot{\rho}_{33} = -\Gamma_R \rho_{33} + \Gamma_L \rho_{22}. \tag{50e}$$

2. Strong interdot Coulomb repulsion

On the other hand, realistic experiments of the double dot are set up in the strong Coulomb blockade regime where not only each of dots has only one effective energy level but also there are no states of simultaneous occupation of the two dots. In other words, the configuration space of the localized charge states in the double-dot system with a strong interdot Coulomb repulsion only contains the states of empty double dot, the first dot occupied, and the second dot occupied, denoted by $|j\rangle, j=0,1,2$, respectively. The corresponding rate equations in this strong Coulomb blockade regime for an arbitrary spectral density can also be obtained by simply excluding the doubly occupied states in Eq. (45). Since the rate of the doubly occupied state $|3\rangle$ in the case of ignoring interdot Coulomb repulsion depends on the populations ρ_{11} and ρ_{22}. This probability flow from states $|1\rangle$ and $|2\rangle$ to $|3\rangle$ should be redirected back into states $|1\rangle$ and $|2\rangle$ in the strong interdot Coulomb repulsion regime. Meanwhile, to ensure the probability conservation without the doubly occupied states, a correction to the dependence of the coherence elements, ρ_{12} and ρ_{21}, in the rate equations for ρ_{11} and ρ_{22} must also be taken into account guided by the condition $\Gamma^{\beta}_{12}\rho_{21}+\Gamma^{\beta}_{21}\rho_{12}-\Gamma^{\beta}_{11}\rho_{22}-\Gamma^{\beta}_{22}\rho_{11}=0$. This condition indeed forces the doubly occupied state to decouple from other states in the double dot as one can see from the rate equation $\dot{\rho}_{33}$ in Eq. (45). These modifications can be done explicitly by taking the following shift to the coefficients in noninteracting rate equation (45):

$$\bar{\Gamma}_{ii} \to \bar{\Gamma}_{ii} + \frac{1}{2}\Gamma^{\beta}_{jj}, \quad \bar{\Gamma}_{ij} \to \bar{\Gamma}_{ij} - \frac{1}{2}\Gamma^{\beta}_{ij}, \tag{51}$$

with $i \neq j$. In fact, the above coefficient shift also automatically cancels the Γ^0 dependence of ρ_{33} in Eq. (45), which is indeed a criterion for entirely excluding the double-occupied state from the reduced density matrix, as one can directly see from the expression of master equation (33). Then the rate equation of ρ_{33} in Eq. (45) becomes $\dot{\rho}_{33}=(-2\ \mathrm{Tr}\ \bar{\Gamma})\rho_{33}$, its solution is $\rho_{33}(t)=0$ if initially $\rho_{33}(t_0)=0$. This implies that no leakage into the double-occupied state will occur. As a result, the rate equations in the strong interdot Coulomb repulsion regime are given by

$$\dot{\rho}_{00} = \tilde{\Gamma}_{11}\rho_{11} + \tilde{\Gamma}_{21}\rho_{12} + \tilde{\Gamma}_{12}\rho_{21} + \tilde{\Gamma}_{22}\rho_{22} + \Gamma^0 \rho_{00}, \tag{52a}$$

$$\dot{\rho}_{11} = -\tilde{\Gamma}_{11}\rho_{11} + \tilde{\Xi}^{*}_{-}\rho_{12} + \tilde{\Xi}_{-}\rho_{21} - \Gamma^{\beta}_{11}\rho_{00}, \tag{52b}$$

$$\dot{\rho}_{22} = -\tilde{\Gamma}_{22}\rho_{22} + \tilde{\Xi}^{*}_{+}\rho_{12} + \tilde{\Xi}_{+}\rho_{21} - \Gamma^{\beta}_{22}\rho_{00}, \tag{52c}$$

$$\dot{\rho}_{12} = \left[-i\varepsilon' - \frac{1}{2}\mathrm{Tr}\ \tilde{\Gamma}\right]\rho_{12} + \tilde{\Xi}_{+}\rho_{11} + \tilde{\Xi}_{-}\rho_{22} - \Gamma^{\beta}_{12}\rho_{00}, \tag{52d}$$

where $\tilde{\Xi}_{\pm}(t) = \pm iT'_c(t) - \frac{1}{2}\tilde{\Gamma}_{12}(t)$. This set of the rate equations depicts the full non-Markovian dynamics of the double dot in the strong interdot Coulomb repulsion regime.

For the case of a constant spectral density in the Markovian limit, $\tilde{\Gamma}_{ij}(t)=[2\Gamma(t)+\Gamma^{\beta}(t)]_{ij} \to \bar{f}_l \Gamma_l \delta_{ij}$, $\tilde{\Xi}_{\pm}(t) \to \pm iT_c$, and $\varepsilon'(t) \to \varepsilon$. The rate equations under such circumstances are reduced to the rate equations for the double dot in the strong interdot Coulomb repulsion regime, given in Ref. 11,

$$\dot{\rho}_{00} = -(f_L\Gamma_L + f_R\Gamma_R)\rho_{00} + \bar{f}_L\Gamma_L\rho_{11} + \bar{f}_R\Gamma_R\rho_{22}, \quad (53a)$$

$$\dot{\rho}_{11} = f_L\Gamma_L\rho_{00} + iT_c(\rho_{12} - \rho_{21}) - \bar{f}_L\Gamma_L\rho_{11}, \quad (53b)$$

$$\dot{\rho}_{22} = f_R\Gamma_R\rho_{00} - iT_c(\rho_{12} - \rho_{21}) - \bar{f}_R\Gamma_R\rho_{22}, \quad (53c)$$

$$\dot{\rho}_{12} = \left[-i\varepsilon - \frac{1}{2}(\bar{f}_L\Gamma_L + \bar{f}_R\Gamma_R)\right]\rho_{12} + iT_c(\rho_{11} - \rho_{22}). \quad (53d)$$

Furthermore, in the large bias limit, $f_L=1$, $f_R=0$, the above rate equations lead to the rate equations of Stoof and Nazarov:[48]

$$\dot{\rho}_{00} = -\Gamma_L\rho_{00} + \Gamma_R\rho_{22}, \quad (54a)$$

$$\dot{\rho}_{11} = \Gamma_L\rho_{00} + iT_c(\rho_{12} - \rho_{21}), \quad (54b)$$

$$\dot{\rho}_{22} = -\Gamma_R\rho_{22} - iT_c(\rho_{12} - \rho_{21}), \quad (54c)$$

$$\dot{\rho}_{12} = \left(-i\varepsilon - \frac{\Gamma_R}{2}\right)\rho_{12} + iT_c(\rho_{11} - \rho_{22}). \quad (54d)$$

In summary, we have derived in this section an exact master equation for the double dot gated by electrodes and corresponding Bloch-type rate equation (45) without considering the interdot Coulomb interaction as well as rate equation (52) for the strong interdot Coulomb repulsion. For convenience, we call Eq. (45) the interaction-free rate equation and Eq. (52) the strong-interaction rate equation hereafter. Other approximated rate equations that have been used in the literature are obtained at well-defined limit of the present formulas.

IV. NON-MARKOVIAN DYNAMICS OF CHARGE QUBIT

With the formulas derived in Sec. III, we can now systematically explore the non-Markovian dynamics of the charge qubit for this double-dot system. The coherence (decoherence) dynamics of electron charges in the double dot is determined by its internal structure as well as external operations. The internal structure includes the spectral properties of the reservoirs as well as the couplings between the dots and the reservoirs embedded in the spectral density. The external operations include charge qubit initialization, its coherence manipulation, and the qubit state readout through the bias controls of the source and drain electrodes. Non-Markovian decoherence effects of these internal structure and external operations to the charge qubit are manifested through the time-dependent coefficients in the master equation, which is completely determined by Eq. (30) after the spectral density $J_{il}(\omega)$ is specified. In fact, the time correlation functions directly tell us the length of the correlation time which determines to what extent the time-dependent fluctuation and memory effect become important. The longer the correlation time is, the more memory effect acts on the electron dynamics in the double dot and vice versa.

To be more specific, we should first specify the spectral density $J_{il}(\omega)$ for the source and drain electrodes. Unlike the bosonic environment where a general spectral density $J(\omega) = \eta\omega(\frac{\omega}{\omega_c})^{n-1}e^{-\omega/\omega_c}$ (ω_c is a high-frequency cutoff and η is a dimensionless coupling constant) was defined and used to classify the bosonic environment as Ohmic if $n=1$, sub-Ohmic if $0<n<1$, and super-Ohmic if $n>1$,[22] for a fermionic environment a general spectral density should not be a Poisson-type or Gaussian-type distribution function because of the Fermi statistics. Here we shall use a Lorentzian spectral density that has been used in the study of the Kondo effect,[34] the influence of a measuring lead on a single dot,[49] and molecular wires coupling to electron reservoirs.[50] The Lorentzian spectral density we used here has a form

$$J_{il}(\omega) = \frac{\Gamma_l d_l^2/2\pi}{(\omega - E_i)^2 + d_l^2}, \quad (55)$$

where E_i is chosen to be the energy levels of the double dot and $l=L,R$ for $i=1,2$, respectively. There are two parameters in $J_{il}(\omega)$ that characterize the time scales of the reservoirs. The parameters $d_{L,R}$ describe the widths of the Lorentzian distributions, which tell how many states in the reservoirs around $E_{1,2}$ effectively involve in the electron tunneling between the reservoirs and dots. Hence, the inverse $d_{L,R}^{-1}$ characterize the time scales of the source and drain electrodes. Another parameter is the electron tunneling strength or the tunneling rate between the reservoirs and dots, $\Gamma_{L,R}$, its inverse characterizes the time scale of the electron tunneling process itself between the reservoirs and dots. Indeed, $\Gamma_{L,R}$ also describe leakage effects of electrons from dots to the reservoirs and vice versa. Thus a Lorentzian spectral density well depict the time scales of non-Markovian processes in this open quantum system.

Also, the choice of a Lorentzian spectral density makes it easy to recover the constant spectral density which has been often used in the literature. In fact, taking the large width limit, namely, assuming all the electron states in the reservoirs have an equal possibility for electron tunneling between the reservoir and dot, then $2\pi J_{il}(\omega) \underset{d_l\to\infty}{\longrightarrow} \Gamma_l$ reproduces the constant spectral density that has often been used in the study of both quantum transport and quantum decoherence phenomena in nanostructures. In this limit, the time scale of the reservoirs is suppressed. Furthermore, in the previous investigations, especially in the study of quantum transport phenomena, one also takes a long-time limit. Combining these two limits (the constant spectral density and long-time limit) together, the exact master equation is reduced to the Bloch-type rate equations in the Markov approximation obtained by other authors,[9,11,48] as we have shown in Sec. III. Hence, with a Lorentzian spectral density, it is not only convenient to analyze in detail the non-Markovian dynamics but also enables us to easily make a comparison with the Markov dynamics.

For a Lorentzian spectral density, the corresponding temperature-independent time correlation function can be exactly calculated. The result is

$$F_{il}(\tau-\tau')=\frac{\Gamma_l d_l}{2}\exp\{-(d_l+iE_i)|\tau-\tau'|\}. \quad (56)$$

Obviously, $d_{L,R}^{-1}$ describes the correlation times of the reservoirs. The wider or narrower it is, the shorter or longer the correlation time will be. The internal structure of the double dot is characterized by the energy-level splitting $\varepsilon=E_1-E_2$ and the interdot tunnel coupling $\Delta=2T_c$, its time scale T_0 is given by the inverse of the bare Rabi frequency $\Omega_0=\sqrt{\varepsilon^2+\Delta^2}$. The non-Markovian dynamics should be dominated when the two typical time scales, Ω_0^{-1} and $d_{L,R}^{-1}$, are in the same order of magnitude. There is another time scale, the reservoirs' temperature $\beta=1/kT$ that also influences the non-Markovian dynamics of the charge qubit in certain cases. In the current experiments for charge qubit manipulation,[4] the temperature is roughly fixed at 100 mK. We will take this temperature throughout our analysis to the charge qubit decoherence.

A. Time-dependent coefficients in the master equation and non-Markovian dynamics

Once the spectral density is specified, the full non-Markovian dynamics of charge qubit in the double dot can be depicted using master equation (33), or more specifically corresponding Bloch-type rate equations (45) and (52) for the cases of no interdot Coulomb repulsion and strong interdot Coulomb repulsion double dot, respectively. To solve the master equation or equivalently the rate equations, we must determine first the time-dependent coefficients contained in these equations, namely, the shifted (renormalized) energy-level splitting $\varepsilon'(t)=E_1'(t)-E_2'(t)$ and interdot tunneling coupling $\Delta'(t)=2T_c'(t)$, as well as the dissipation-fluctuation coefficients $\Gamma(t)$ and $\Gamma^\beta(t)$. These transport coefficients are completely determined by the functions $u(t)$ and $v(t)$ as the solutions of dissipation-fluctuation equation of motion (30) which has to be solved numerically for a given spectral density.

Using the Lorentzian spectral density [Eq. (55)], we can calculate explicitly all the time-dependent transport coefficients in the master equations and then discuss the corresponding non-Markovian dynamics by comparing with the Markovian limit in various different time scales. We shall first analyze the time-dependent coefficients for the charge qubit initialization where a bias is applied to the double dot and the double dot is adjusted to be off-resonance, i.e., $eV_{\rm SD}=\mu_L-\mu_R\neq 0$ and $\varepsilon=E_1-E_2\neq 0$.[4] We will examine when the large bias limit is reached and how the initialization works. After that we will go to the coherent manipulation regime where the double dot is set up symmetrically ($E_1=E_2$) and the chemical potentials of the electron reservoirs are aligned above the energy levels of two dots with zero-bias voltage ($\mu_L=\mu_R$). The time dependence of $\varepsilon'(t), T_c'(t)$ as well as $\Gamma(t)$ and $\Gamma^\beta(t)$ in this regime will tell us when the non-Markovian dynamics becomes important during the charge qubit evolution.

Dissipation-fluctuation equation of motion (30) shows that only the solution of $v(t)$ depends on the Fermi distribution function in the reservoirs. In other words, only $\Gamma^\beta(t)$ sensitively depends on the bias. Other coefficients, $\varepsilon'(t)$, $T_c'(t)$, and $\Gamma(t)$, do not depend on the chemical potentials $\mu_{L,R}$ and thus the bias. Their time dependencies are completely determined by the internal parameters of the double dot and the spectral density. In the initialization scheme where a bias is presented and the energy splitting of the two levels in the double dot is nonzero within the transport window, the time dependence of Γ^β is plotted in Fig. 3 by varying the bias voltage. We find that the large bias limit is reached at about 100 μeV for the given internal parameters: $\varepsilon=30$ μeV, $\Delta=10$ μeV, $\Gamma_{L,R}=\Delta$, and $d_{L,R}=\Delta/2$, with $\Omega_0=\sqrt{\varepsilon^2+\Delta^2}\simeq 32$ μeV being the bare Rabi frequency of the charge qubit. This large bias limit in Fig. 3 shows that the curves for $eV_{\rm SD}=90$ μeV are very close to the curves of $eV_{\rm SD}=430$ μeV, and the curves for $eV_{\rm SD}=130$ μeV perfectly overlap with the curves of $eV_{\rm SD}=430$ μeV.

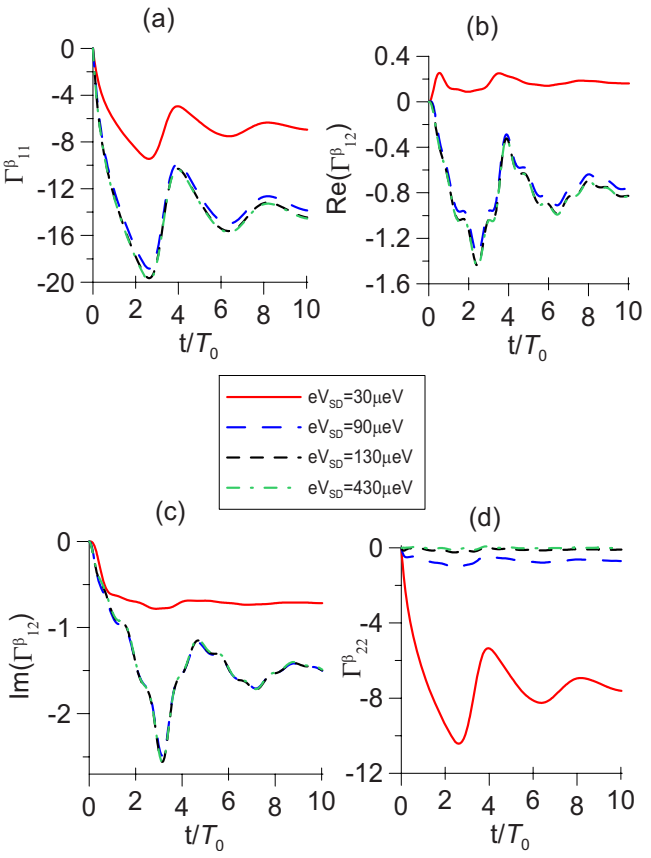

FIG. 3. (Color online) The time dependence of Γ^β by varying the bias voltage. The double dot is set to be off-resonance with $\varepsilon=30$ μeV, $\Delta=10$ μeV, $\Gamma_{L,R}=\Delta$, and $d_{L,R}=\Omega_0/2$. (a) and (d) show the two diagonal matrix elements of Γ^β. Since Γ^β is Hermitian only one of the off-diagonal elements is plotted with the real part shown in (b) and the imaginary part in (c). The period of the bare Rabi cycle is $T_0=2\pi/\Omega_0$.

Figure 4 shows the time dependence of other coefficients for different energy-level splitting of the double-dot states ($\varepsilon=0,10,70$ μeV) with different tunneling rates ($\Gamma_L=\Gamma_R=2.5,10,25$ μeV). The result shows that $\varepsilon'(t)=0$ for $\varepsilon=0$, and the initial value $\mathrm{Re}(T_c')(0)$ is always equal to T_c with $\mathrm{Im}(T_c')(0)$ being zero in all the cases we have calculated. For a small tunneling rate ($\Gamma_{L,R}<\Delta/2$), the time dependence of

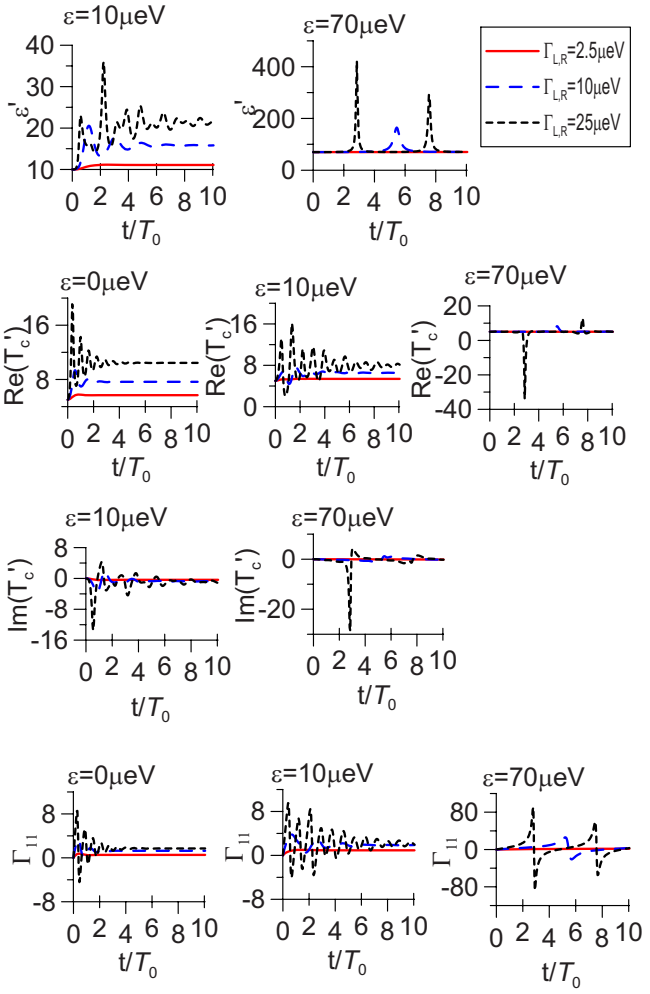

FIG. 4. (Color online) The time dependence of the coefficients $\varepsilon'(t)$, $T_c'(t)$, and $\Gamma(t)$ for different energy splitting ε and tunneling rate $\Gamma_{L,R}$ at the interdot coupling $\Delta=10$ μeV and the spectral widths $d_{L,R}=\Delta/2$.

these coefficients is almost negligible (see red solid lines in Fig. 4). The time-dependent effect appears when the tunneling rates between the reservoirs and dots become relatively large. These time-dependent behaviors vary sensitively on the energy splitting of the double-dot states. Increasing the energy splitting ε changes the time-dependent behaviors of all the coefficients significantly, as shown in Fig. 4.

The dynamics of electron charges in this initialization regime is plotted in Fig. 5. If we dope only one excess electron in the left dot with the right dot being empty, the efficiency of keeping this initial state decreases as the bias decreasing [see Fig. 5(a)]. If the two levels of the double dot are in resonance ($\varepsilon=0$) or the interdot tunnel coupling is larger than the tunneling rates $\Delta>2\Gamma_{L,R}$, it also has a low efficiency to keep the double dot in the initial state $\rho_{11}=1$. A large bias configuration (eV_{SD} larger than 100 μeV) maintains the double dot in the initial state $\rho_{11}=1$ very well. Furthermore, for a large bias it also quickly leads the double dot into the state $\rho_{11}\sim 1$ even if the initial state is $\rho_{00}=1$ (both dots are empty initially) or $\rho_{22}=1$ (the left dot is empty but the right dot is occupied by one excess electron), as shown in Fig. 5(b). These numerical solutions are obtained using

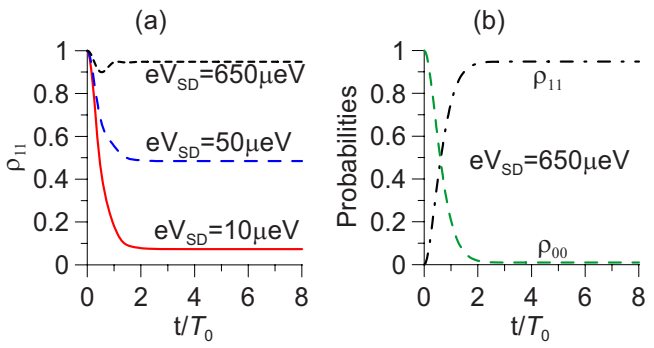

FIG. 5. (Color online) (a) The time evolution of ρ_{11}, the probability of finding one excess electron in the left dot with the right dot being empty, is plotted at various bias when the initial state is $\rho_{11}=1$. (b) The time evolutions of ρ_{11} (black dash-dotted line) and ρ_{00} (green long-dashed line) when the initial state is an empty state ($\rho_{00}=1$), where $eV_{\mathrm{SD}}=650$ μeV. Other input parameters used here are the same as that in Fig. 3.

interaction-free rate equation (45). But strong-interaction rate equation (52) gives qualitatively the same result for initialization. Taking the bias to be 650 μeV and the reservoirs' temperature to be 100 mK that have used in experiments,[4] a very efficient initialization of the charge qubit can be obtained, as shown in Fig. 5.

Meanwhile, Fig. 4 shows that for a relatively large tunneling rate $\Gamma_{L,R}$, the smooth time oscillation of all the coefficients at small ε become discontinuing at a relatively large ε value. Such discontinuities correspond to the electron hopping to the localized charge states in the double dot where the interdot tunnel coupling Δ is almost negligible in comparison with the level splitting ε. Such discontinuities are also manifested perfectly in the electron dynamics. The discontinuities coincide with the times at which the electron is found in a localized charge state of the double dot in a very high probability. Figures 6(a) and 6(b) are obtained using rate equations (45) and (52), respectively, where we plot the corresponding electron charge dynamics together with the time dependence of Γ_{11}. We find that for a large bias, the electron charge dynamics given by interaction-free rate equation (45) and strong-interaction rate equation (52) display the same feature, including the coincidence between the discontinuities in the time-dependent coefficients and the emergence of a localized charge state in the double dot. Note that if a sufficiently large bias is applied across the double dot, initialization can still be achieved regardless of these discontinuities. This is because a large bias is the most dominant factor in this situation. As a conclusion, initialization of charge qubit in the double dot can be easily achieved in a large bias limit with relatively small tunnel coupling and tunneling rates. All these parameters are tunable in experiments.

Now we turn into the regime for charge qubit rotations where the double dot is set up at the resonant levels ($E_1=E_2=E$) and the Fermi surfaces of the electron reservoirs are aligned above the resonant levels ($\mu_L=\mu_R=\mu$ and $\mu-E>0$). In other words, the double dot is set to be symmetric and unbiased for charge coherence manipulation.[4] Figures 7–9 show the time dependencies of the shifted interdot tunnel

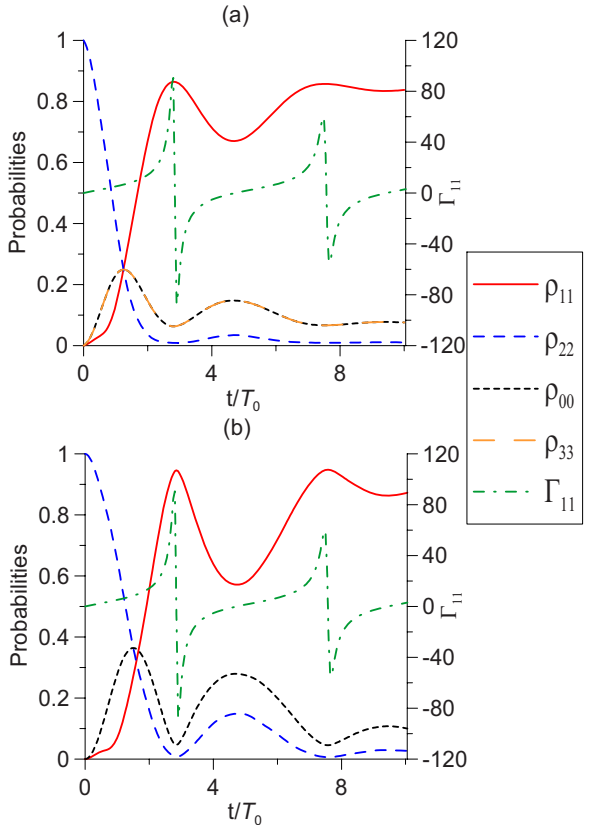

FIG. 6. (Color online) The coincidence between the discontinuities in $\Gamma_{11}(t)$ (the green dot-dashed line) and the emergence of a localized charge state in the double dot. The input parameters $\varepsilon=70$ μeV, $\Delta=10$ μeV, $d_{L,R}=\Delta/2$, and $\Gamma_{L,R}=25$ μeV with the bias $eV_{SD}=120$ μeV such that the initialization can be achieved. (a) For the double dot without considering the interdot Coulomb repulsion. (b) For the double dot in the strong interdot Coulomb repulsion regime.

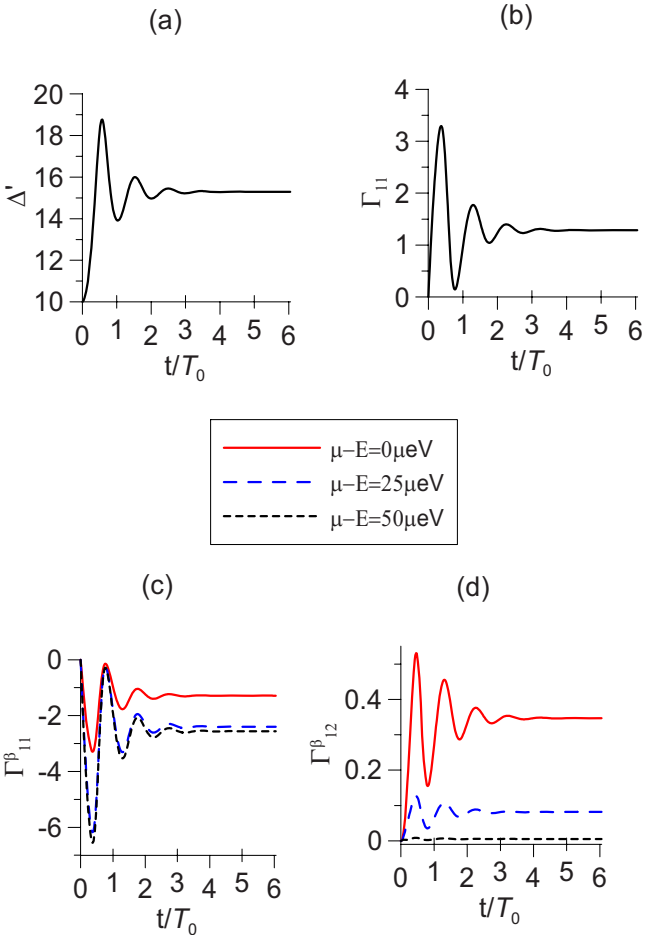

FIG. 7. (Color online) (a) The shifted interdot tunnel coupling $\Delta'(t)$ and [(b)–(d)] the dissipation-fluctuation matrix elements, $\Gamma_{11}(t)$ and $\Gamma^{\beta}_{11,12}(t)$, by varying the chemical potential $\mu=\mu_{L,R}$. The dot parameters $E=E_1=E_2$ and $\Delta=10$ μeV. $\Gamma_{L,R}=\Delta$ and $d_{L,R}=\Delta/2$. The matrix Γ^{β} is Hermitian so that only one of the off-diagonal elements is presented here. The red solid, blue long–dashed, and the black short-dashed lines correspond to $\mu-E=0$, 25, and 50 μeV, respectively.

coupling $\Delta'(t)$, as well as the dissipation-fluctuation matrices $\Gamma(t)$ and $\Gamma^{\beta}(t)$ for the symmetric double dot by varying the chemical potential $\mu-E$, the spectral widths $d_{L,R}$, and the tunneling rates $\Gamma_{L,R}$, respectively, from which we can determine the time scales within which non-Markovian processes dominate the charge coherence dynamics at zero bias. We find that for the symmetric double dot, the shifted energy-level splitting $\varepsilon'(t)$, and the imaginary part of the shifted interdot tunnel coupling Im $\Delta'(t)$ are kept to be zero as we have already pointed out in Fig. 4. The off-diagonal element $\Gamma_{12}(t)$ and the imaginary part of $\Gamma^{\beta}_{12}(t)$ are found also to be zero, while the diagonal elements $\Gamma_{11}(t)=\Gamma_{22}(t)$ and $\Gamma^{\beta}_{11}(t)=\Gamma^{\beta}_{22}(t)$. All the time-dependent coefficients change in time in the beginning and then approach to an asymptotic value (the Markovian limit) at different time scales. These time-dependence behaviors will be used to analyze the decoherence dynamics of charge qubit in Sec. IV B.

In Fig. 7 we plot the shifted interdot tunnel coupling $\Delta'(t)$, the dissipation-fluctuation matrices $\Gamma_{11}(t)$ and $\Gamma^{\beta}_{11,12}(t)$ by varying the chemical potentials with respect to the energy levels of the double dot, $\mu-E$. The red solid, blue long-dashed, and the black short-dashed lines correspond to $\mu-E=0$, 25, and 50 μeV respectively. In Fig. 7 the spectral widths $d_{L,R}=\Omega_0/2$, where $\Omega_0=\Delta$ is the bare Rabi frequency of the double dot. In other words, the time scale of the reservoirs is chosen about two Rabi cycles of the system. A large amplitude variation in these time-dependent coefficients within the time scale of the reservoirs is clearly shown in the figure. After that time, all these time-dependent coefficients approach to a steady value which corresponds to their asymptotic values as a Markovian limit. This indicates that the possible non-Markovian dynamics is mainly caused by the time fluctuations of these coefficients within the characteristic time of the reservoirs.

Figure 8 is the same plot with varying the electron tunneling rates between the reservoirs and dots but fixing the chemical potentials at $\mu-E=\Delta$. The small tunneling rate $\Gamma_{L,R}=2.5$ μeV ($\leq\Delta/2$) does not show a significant time variation in the dissipation-fluctuation coefficients, as also shown in Fig. 4. The shifted interdot tunnel coupling at this tunneling rate is very close to the bare one ($\sim\Delta$); see the red solid line in Fig. 8(a). This implies that a small electron

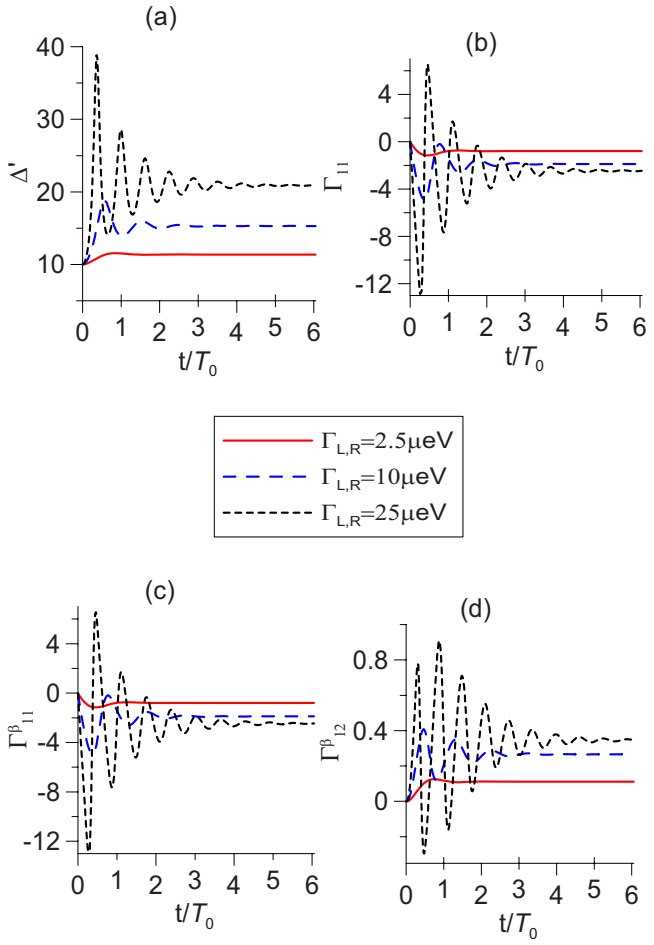

FIG. 8. (Color online) The same plot as in Fig. 7 with fixing the chemical potentials at $\mu - E = \Delta$ and varying the electron tunneling rates between the reservoirs and dots $\Gamma_{L,R}$ symmetrically. The other parameters are the same as in Fig. 7.

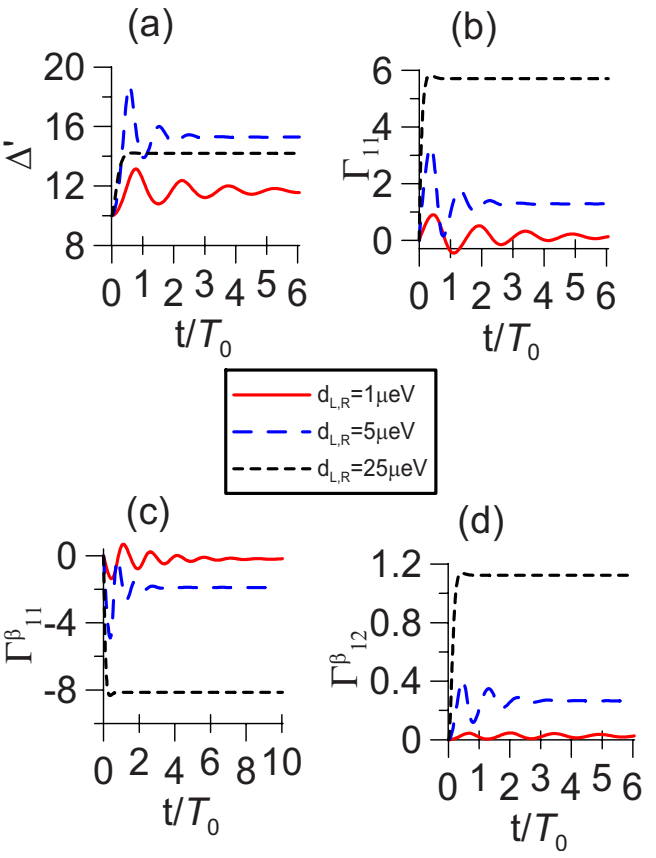

FIG. 9. (Color online) The same plot as in Fig. 8 by varying $d_{L,R}$ but fixing $\Gamma_{L,R} = \Delta$ and other parameters are those used in Fig. 8.

tunneling rate between the reservoirs and dots (corresponds to a small leakage effect) does not manifest the non-Markovian dynamics significantly. Increasing the tunneling rates enlarges the charge leakage effect from the reservoirs to dots and vice versa, thus enhances the non-Markovian effects as well, as shown by the giggling and wiggling time evolutions of the dissipation-fluctuation coefficients in the figure. The time dependence of shifted interdot tunnel coupling Δ' at large tunneling rates also has a significant shift from the bare one Δ besides the oscillation within the non-Markovian time region. Meanwhile, the charge oscillation frequency has different shifts from the bare Rabi frequency for different $\Gamma_{L,R}$ values. How these time-dependent (non-Markovian) behaviors influencing the charge coherence will be discussed in detail in Sec. IV B.

Figure 9 shows how the time dependence of the shifted interdot tunnel coupling and the dissipation-fluctuation coefficients change by varying the spectral widths $d_{L,R}$. We plot these time-dependent coefficients for three different spectral widths: $d_{L,R}=1$, 5, and 25 μeV. The result shows that when $d_{L,R}=25$ μeV, the dynamics of the double dot already reaches to the Markovian limit, namely, all the time-dependent coefficients approach their asymptotic values in a very short time (less than a half cycle of the bare Rabi oscillation). When the spectral widths $d_{L,R}$ becomes small ($\leq\Delta$) so that the characteristic time of the reservoirs becomes long), the time oscillation of all the transport coefficients becomes strong. Correspondingly the charge dynamics is dominated by non-Markovian processes.

The above numerical results tell that the spectral widths $d_{L,R}$ of the reservoirs (mainly as a memory effect) and the tunneling rates $\Gamma_{L,R}$ between the reservoirs and dots (mainly as a leakage effect) are two basic parameters for characterizing the occurrence of non-Markovian dynamics in this double-dot device. Comparing the results in Figs. 7–9, we find that for the coherence manipulation of charge qubit where the double dot is unbiased,[4] the time for the dissipation-fluctuation coefficients reaching a steady limit depends on the spectral widths of the tunneling spectra as well as the tunneling rates between the reservoirs and dots. The Markovian limit often used in the literature is valid for the electron reservoirs having a relatively small tunneling rate (negligible leakage effect) and a large spectral width (negligible memory effect). The former implies the validity of the Born approximation and the latter corresponds to the Markov approximation. The chemical potentials of the electron reservoirs controlled by the external bias voltage just modifies the values of the dissipation-fluctuation coefficients Γ^{β} without altering the characteristic times of the reservoirs and the system, as shown in Figs. 3 and 7. However, the chemical potential can be very efficient in suppressing the

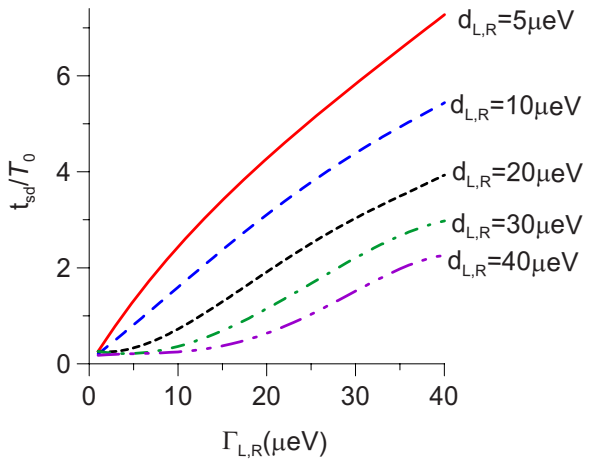

FIG. 10. (Color online) The lines for separating the Markovian and the non-Markovian dynamics in the $\Gamma_{11}-t$ plot; each line corresponds to a given value of $d_{L,R}$. The parameters $\mu-E=\Delta=10\ \mu$eV are used.

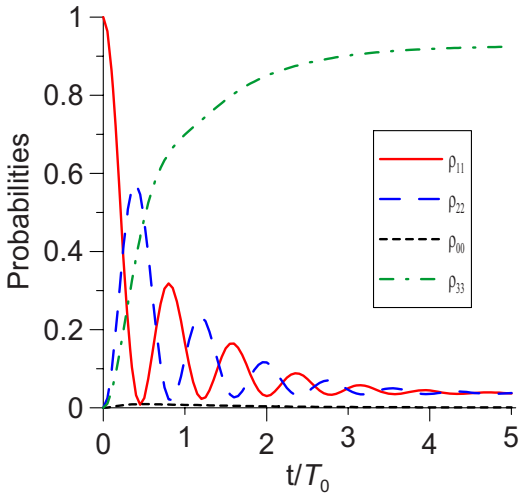

FIG. 11. (Color online) The time evolutions of the populations ρ_{11} (the red solid line), ρ_{22} (the blue long-dashed line), ρ_{00} (the black short-dashed line), and ρ_{33} (the green dashed-dotted line) calculated using interaction-free rate equation (45) in the symmetric double dot with $\Delta=10\ \mu$eV, $\mu-E=30\ \mu$eV, $d_{L,R}=\Delta/2$, and $\Gamma_{L,R}=d_{L,R}$. Without considering the interdot Coulomb repulsion, raising up of the chemical potentials $\mu>E$ accumulates charges into the double dot.

leakage effect. Thus, $\mu-E$ is a competitive control parameter in the coherence control of charge qubit, as we will see later.

In order to show clearly when non-Markovian or Markovian processes play a major role in charge qubit decoherence, we take Γ_{11} as an example to examine at what time this dissipation-fluctuation coefficient reaches its steady value by varying $d_{L,R}$ and $\Gamma_{L,R}$. The result is plotted in Fig. 10. The lines signify transition times between the time-dependent fluctuating and the steady dissipation-fluctuation coefficients by varying tunneling rate at a given spectral width. Non-Markovian dynamics can be seen mostly in the time range under the lines. It shows that the strong non-Markovian dynamics corresponds to a relatively small spectral widths $d_{L,R}$ (a strong memory effect) and a relatively large tunneling rates $\Gamma_{L,R}$ (a large leakage effect) compared with the interdot tunnel coupling Δ. Non-Markovian dynamics disappears for a large $d_{L,R}$ ($\geq 2\Delta$) and a small $\Gamma_{L,R}$ ($\leq\Delta/2$). In the parameter range of interest to the experiments,[1] the non-Markovian processes do not go over more than five Rabi cycles, with which a significant effect can be seen in maintaining charge coherence, as we will see below.

B. Decoherence dynamics of charge qubit

Having examined the time dependencies of all the transport coefficients [the shifted energy-level splitting $\varepsilon'(t)$, the renormalized interdot tunnel coupling $\Delta'(t)$, and the dissipation-fluctuation coefficients $\Gamma(t),\Gamma^{\beta}(t)$] in the master equation for both biased and unbiased double dots, we shall discuss now the decoherent dynamics of the charge qubit in this section. Experimentally the coherence manipulation of charge qubit is performed for the double dot on-resonance, $\varepsilon=E_1-E_2=0$. The corresponding shifted energy-level splitting $\varepsilon'(t)$ remains zero. Then the energy eigenbasis of the charge qubit refers actually to the molecular antibonding and bonding states, namely, $|\pm\rangle\equiv\frac{1}{\sqrt{2}}(|1\rangle\pm|2\rangle)$. The oscillation between the coherently coupled localized charge states $|1\rangle$ and $|2\rangle$ as coherent superpositions of the molecular states describes the charge coherence, where the renormalized Rabi frequency $\Omega(t)=\Delta'(t)$ is just the shifted interdot tunnel coupling for the symmetric double dot. The time-dependent dissipation-fluctuation coefficients $\Gamma(t),\Gamma^{\beta}(t)$ will disturb this coherent oscillation and cause charge qubit decoherence.

To be specific, we let the initial state be $\rho_{11}=1$ and examine the time evolution of the density matrix under various conditions. First we calculate rate equation (45) for the no-Coulomb-interacting double dot. The typical population evolution shown in Fig. 11 tells that the double occupancy is favored. In fact, the charge qubit of a double dot is designed in the strong interdot Coulomb blockade regime where the state of simultaneous occupation of two dots is excluded. In other words, unlike the charge qubit initialization where both the interaction-free and the strong interaction rate equations give qualitatively the same result, for the coherence control of the charge qubit, interaction-free rate equation (45) is invalid. The charge qubit dynamics must be described by strong-interaction rate equation (52). For rate equation (52) in the strong interdot Coulomb repulsion regime to be held for charge qubit manipulation, the energy difference between the Fermi surfaces of the reservoirs and the energy levels of the dots, $\mu-E$, cannot be too large. The interdot Coulomb repulsion in the samples is estimated to be 200 μeV.[4] The value of $\mu-E$ that can be taken most safely should be not larger than 50 μeV, a quarter of the interdot Coulomb repulsion energy. If $\mu-E$ is taken over 100 μeV, it is comparable to the Coulomb repulsion energy so that the doubly occupied state cannot be completely excluded. For convenience and consistency with the discussion in Sec. IV A, we still take the quantum dot parameters $E_1=E_2=E$ and $\Delta=10\ \mu$eV. As one will see with $\mu-E=25\sim 50\ \mu$eV, with $\Gamma_{L,R}$ and $d_{L,R}$ being in a reasonable range, the charge qubit can maintain coherence very well.

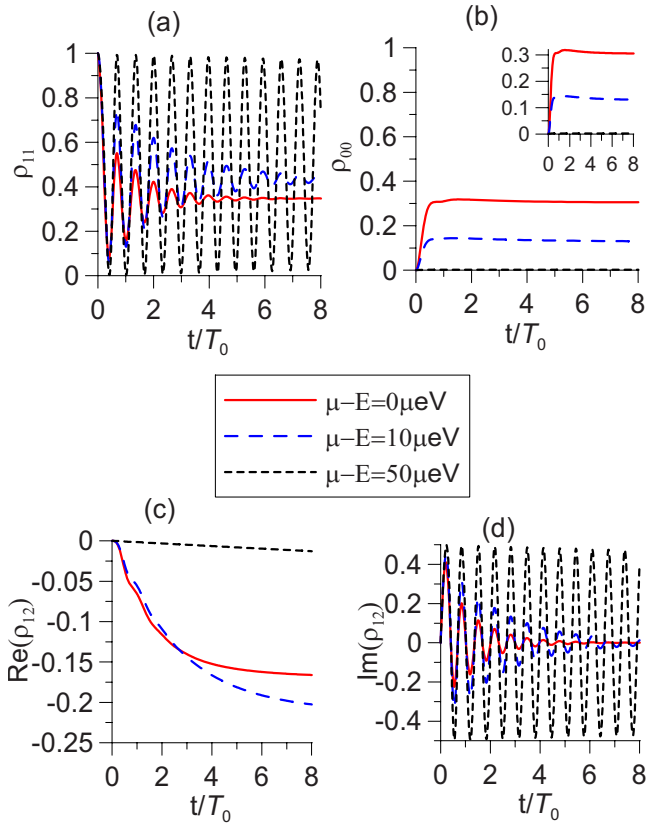

FIG. 12. (Color online) The time evolutions of the density matrix at different $\mu-E$ with E fixed. The red solid line is for $\mu-E=0$, the blue long-dashed line is for $\mu-E=10$ μeV, and the black short-dashed line is for $\mu-E=50$ μeV. $d_{L,R}=\Delta/2$ and $\Gamma_{L,R}=\Delta$.

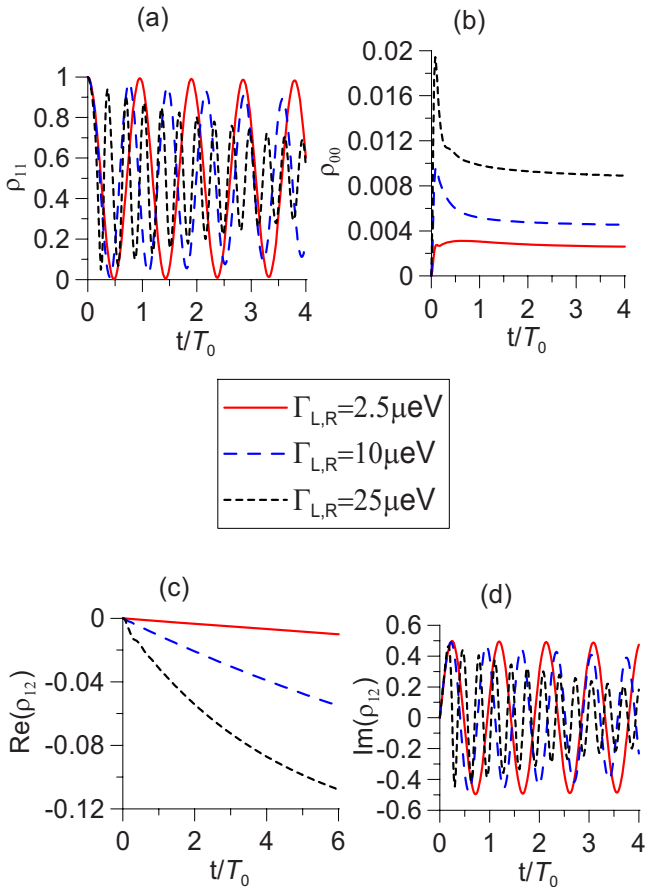

FIG. 13. (Color online) The time evolutions of the density matrix at different coupling constants. The red solid line is for $\Gamma_{L,R}=2.5$ μeV, the blue long-dashed line is for $\Gamma_{L,R}=10$ μeV, and the black short-dashed line is for $\Gamma_{L,R}=25$ μeV. The chemical potentials are kept at $\mu-E=50$ μeV and $d_{L,R}=25$ μeV.

In Fig. 12, we plot the time evolution of the reduced density matrix by varying the aligned Fermi surfaces. The result shows that the coherent oscillation of the charge qubit depends sensitively on the height of aligned Fermi surfaces from the resonant levels of the double dot, i.e., $\mu-E$. When $\mu-E$ is not too large ($<\Delta$) and $\Gamma_{L,R}$ is not too small ($>\Delta$), the population ρ_{11} decays very quickly. This is because although the state of simultaneous occupation of two dots is excluded, there is still chance for electrons to escape from the dots into the reservoirs such that both dots become empty, namely, $\rho_{00}\neq 0$ [see Fig. 12(b)] as a leakage effect. This effect can be suppressed when the Fermi surfaces are aligned such that $\mu-E$ must be relatively larger than $\Gamma_{L,R}$. As a result, the charge qubit can maintain the coherence very well. In Fig. 12(a), we see that the charge coherence is perfectly maintained for $\mu-E=50$ μeV. Meanwhile, the real and the imaginary parts of the off-diagonal density-matrix element ρ_{12} exhibit quite different dynamics. The imaginary part of ρ_{12} has a similar oscillatory feature as ρ_{11} [see Fig. 12(d)], which depicts the coherent tunnel coupling between two dots. While the real part of ρ_{12} goes down to be negative [see Fig. 12(c)] which is related to the loss of the energy (dissipation). We find that to maintain a good coherent dynamics for charge qubit, the Fermi surfaces of the reservoirs is better to be aligned above the energy levels of the double dot not less than 2Δ.

In Fig. 13 we plot the time evolution of the reduced density matrix at a few different tunneling rates but fixing other parameters. Experimentally, the tunneling rates between the dots and the reservoirs are also tunable. We fixed the spectral widths at $d_{L,R}=25$ μeV for which the memory effect is largely suppressed. Meantime, we take $\mu-E=50$ μeV (much larger than $\Gamma_{L,R}$) such that the leakage effect is also largely suppressed. When the tunneling rates are small ($<\Delta/2$), the time dependence of these transport coefficients in the master equation are negligible (as shown in Fig. 8) so that no non-Markovian dynamics can be observed. The corresponding charge dynamics is given by the red solid lines in Fig. 13 where the oscillation frequency is time independent, consistent with the result in Markov approximation. When the tunneling rates become large ($\geq\Delta$), the charge frequency is largely shifted and varies in time. The larger the tunneling rates are, the faster the electron oscillates between two dots and the reservoirs, thus the stronger the non-Markovian dynamics occurs. Here the decay of the coherent charge oscillation (see the blue long-dashed and black short-dashed lines in Fig. 13) is not due to the charge leakage (which has been mainly suppressed by raising up the Fermi surfaces) but to a backreaction decoherence effect of the reservoirs when the tunneling rate becomes larger. Increasing the tunneling rates leads to more charge leakage. However, comparing the magnitude of ρ_{00} with that of ρ_{11} shows that the damping of

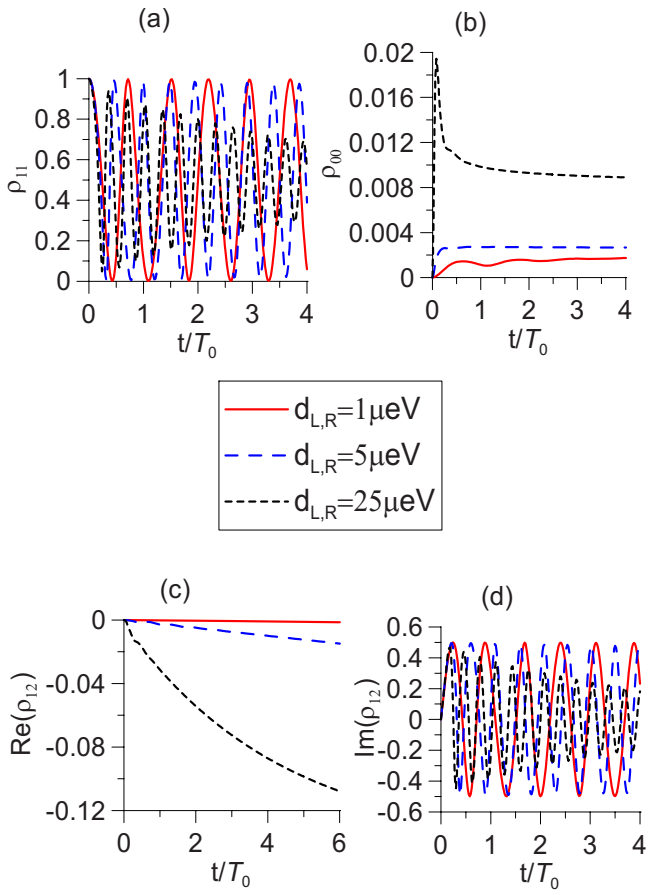

FIG. 14. (Color online) The time evolutions of the density matrix at different spectral widths. The red solid line is for $d_{L,R}=1$ μeV, the blue long-dashed line is for $d_{L,R}=5$ μeV, and the black short-dashed line is for $d_{L,R}=25$ μeV. $\mu-E$ is kept at 50 μeV and $\Gamma_{L,R}=\Delta$.

coherent charge oscillation in the presence of a large tunneling rate is not primarily due to charge leakage but a non-Markovian backreaction decoherence effect.

The more non-Markovian dynamics can be seen by varying the spectral widths $d_{L,R}$. When the spectral width is comparable to the interdot coupling Δ, namely, the characteristic time of reservoirs is comparable to the characteristic time of the double dot, the non-Markovian dynamics becomes the most significant in the time evolution of charge coherence. Although it is currently not clear how to tune the spectral widths in experiments, it is still interesting to see what roles the spectral widths (or more generally speaking, a nonconstant spectral density) play in the charge decoherence dynamics. We plot in Fig. 14 the time evolutions of the density-matrix elements at various spectral widths with $\mu-E=50$ μeV and $\Gamma_{L,R}=\Delta$. As we can see if $d_{L,R}$ is small ($\leq\Delta/2$), the coherent charge dynamics is well preserved although it is a strong non-Markovian process. With increasing the spectral widths, the decoherent charge dynamics becomes visible and also becomes Markov type. Widening the spectral widths damps the coherent charge oscillation. Wider spectral width also causes more charge leakage. But comparing the magnitudes of ρ_{00} with ρ_{11} in Fig. 14 shows again that the damping of coherent charge oscillation in the presence of a wide spectral width is a Markovian decoherence effect. The frequencies of coherent charge oscillation are also shifted differently from the bare Rabi frequency for different spectral widths presented [see Figs. 14(a)–14(d)].

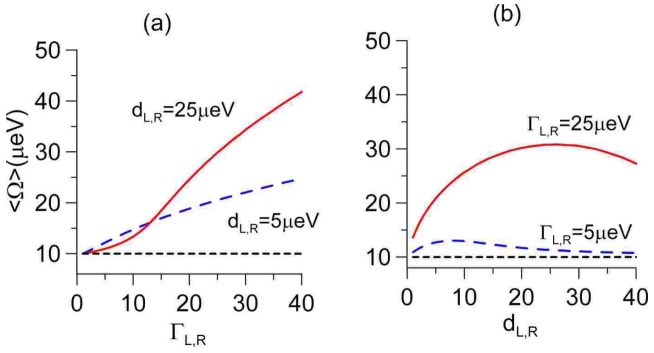

FIG. 15. (Color online) The average renormalized Rabi frequency $\langle\Omega\rangle=\bar{\Omega}(t)$ by varying the spectral widths $d_{L,R}$ and the tunneling rate $\Gamma_{L,R}$, respectively, and comparing with the bare Rabi frequency (the black short-dashed lines). Here we take $\mu-E=50$ μeV to suppress the charge leakage.

From the above analysis, we find that the charge qubit coherence can be maintained very well when either the spectral widths $d_{L,R}$ or the tunneling rates $\Gamma_{L,R}$ are sufficiently smaller than $\mu-E$. However, when both the spectral widths $d_{L,R}$ and the tunneling rates $\Gamma_{L,R}$ become comparable to $\mu-E$, the decay of charge coherency can be seen within a few cycles of the bare Rabi oscillation. The difference between the non-Markovian and the Markovian process manifests in the difference between the renormalized Rabi frequency $\Omega(t)=\Delta'(t)$ (for the symmetric double dot) and the bare Rabi frequency $\Omega_0=\Delta$. In Fig. 15, we plot the average renormalized Rabi frequency $\langle\Omega\rangle=\bar{\Omega}(t)$ by varying the spectral widths $d_{L,R}$ and the tunneling rate $\Gamma_{L,R}$, respectively, and make a comparison with the bare Rabi frequency (the black short-dashed lines). It shows that the renormalized Rabi frequency has a large shift from the bare one, except for the region (the Markov regime) with the spectral width $d_{L,R}>2\Delta$ and the tunneling rate $\Gamma_{L,R}<\Delta/2$, where the renormalized Rabi frequency is close to the bare one. In Fig. 16, we plot the time evolution of density matrix ρ_{11} using strong-interaction rate equation (52) for a few different sets of $(\Gamma_{L,R},d_{L,R})$ and make a comparison with the Markovian approximation determined by rate equation (53), where the charge coherence dynamics in the double dot from Markovian to the non-Markovian processes is clearly demonstrated.

C. Relaxation time T_1 and dephasing time T_2

To understand quantitatively the decoherence dynamics of charge qubit in the double dot, we shall now extract the decay rates (the relaxation time T_1 and the dephasing time T_2) for various manipulation conditions. The relaxation time T_1 characterizes the time going from the antibonding state (with higher energy) to the bonding state (with lower energy) in the energy eigenbasis $|\pm\rangle=\frac{1}{\sqrt{2}}(|1\rangle\pm|2\rangle)$ (for symmetric double dot). It is described by the decay of the diagonal element of the density matrix in the energy eigenbasis,

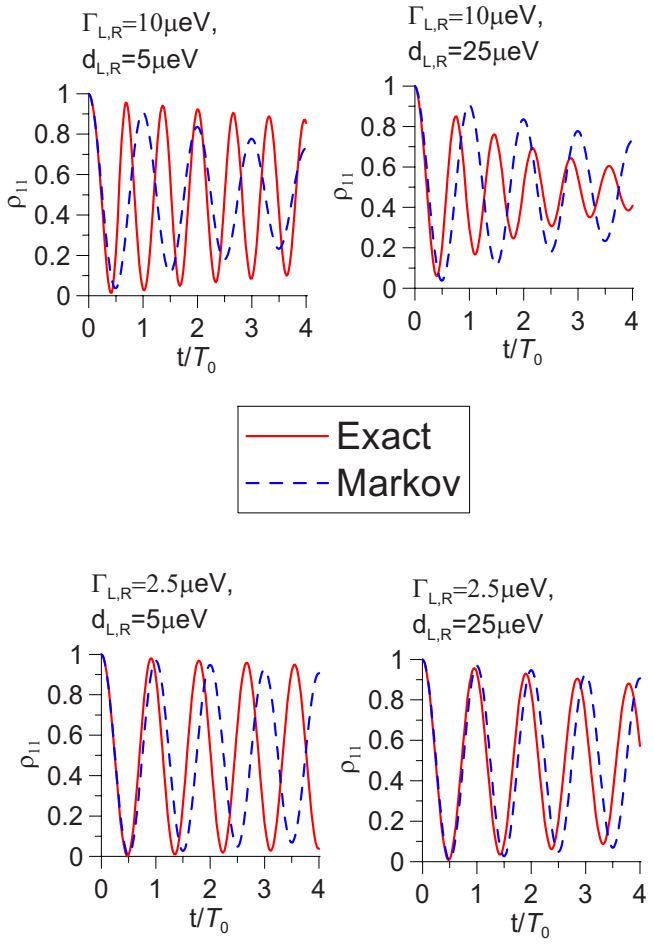

FIG. 16. (Color online) The time evolutions of ρ_{11} obtained from rate equation (52) and the corresponding Markovian limit [Eq. (53)] for the strong-Coulomb-interacting double dot. (a) The strongest non-Markovian regime for a small spectral width and a large tunneling rate. (b) The non-Markovian dynamics controlled by a large tunneling rate alone. (c) The non-Markovian dynamics controlled by a small spectral width alone. (d) The Markov regime corresponding to a small tunneling rate and large spectral width. Here we take $\mu - E = 30\ \mu$eV.

$\langle +|\rho|+\rangle = \frac{1}{2}(\rho_{11}+\rho_{22}) + \mathrm{Re}(\rho_{12})$. In the ideal case (such as in NMR), $\rho_{11}+\rho_{22}=1$ so that T_1 is completely determined by the real part of ρ_{12}. For the charge qubit in double dots, in general $\rho_{11}+\rho_{22}<1$ because of charge leakage. But in the practical manipulation, the Fermi surfaces of the reservoirs are set high enough from the resonant energy levels of the double dot such that charge leakage can be suppressed. Thus we can still extract T_1 from Re ρ_{12}. The decoherence (dephasing) time T_2 corresponds to the decay of the off-diagonal element of the reduced density matrix $\langle +|\rho|-\rangle = \frac{1}{2}(\rho_{11}-\rho_{22}) - i\ \mathrm{Im}(\rho_{12})$. As we will see later the time dependencies of ρ_{11}, ρ_{22} and the imaginary part of ρ_{12} behave very similarly. This may tell us that T_2 can be extracted from either ρ_{11}, ρ_{22} or Im ρ_{12}. Experimentally, one extracted T_2 from ρ_{22} by measuring the current proportion to ρ_{22}.[4]

Having made the above analysis, we shall extract the decay rates of the charge coherent oscillations from the time evolution of the reduced density-matrix elements Re $\rho_{12}(t)$ and Im $\rho_{12}(t)$ or $\rho_{11}(t)$ by fitting a decay oscillating function plus an offset to the numerical data. An intuitive fitting function for the charge oscillation decay would be $Ae^{-Bt}\cos(\langle\Omega\rangle t) + C$. However this fitting function fails for $\rho_{11}(t)$. The typical damping oscillation of $\rho_{11}(t)$ shows that it converges to a steady value of $\rho_{11} \leq \frac{1}{2}$ at large t. Thus $\rho_{11}(t)$ can be well described by the fitting function

$$\rho_{11}(t) = f_h(t)\cos^2(\langle\Omega\rangle t/2) + f_l(t)\sin^2(\langle\Omega\rangle t/2), \qquad (57)$$

where $f_{h,l}(t) = A_{h,l}\exp(-B_{h,l}t^s) + C_{h,l}$ are used to fit the downward shift of the peaks and the upward shift of the valleys in the damped oscillation, respectively. The oscillating function is the squares of sine and cosine functions with half the oscillation frequency, $\sin^2(\langle\Omega\rangle t/2)$ and $\cos^2(\langle\Omega\rangle t/2)$, rather than $\cos(\langle\Omega\rangle t)$ and $\sin(\langle\Omega\rangle t)$. This can be easily understood by considering an ideal qubit. Its Rabi oscillation conditioned to the initial state $\rho_{11}(0)=1$ is given by

$$\rho(t) = \begin{pmatrix} \cos^2\left(\frac{\Omega t}{2}\right) & -\frac{i}{2}\sin(\Omega t) \\ \frac{i}{2}\sin(\Omega t) & \sin^2\left(\frac{\Omega t}{2}\right) \end{pmatrix}$$

in the localized charge state basis. Similarly, the off-diagonal density-matrix elements can be described by the fitting functions,

$$\mathrm{Im}\ \rho_{12}(t) = \{A_i\exp(-B_i t^s) + C_i\}\sin(\langle\Omega\rangle t), \qquad (58a)$$

$$\mathrm{Re}\ \rho_{12}(t) = A_r\exp(-B_r t^s) + C_r. \qquad (58b)$$

The fitting parameters A_x, B_x, C_x for $x = h, l, i, r$ are generally different for different fitting function and data. Figure 17 is a plot of using the fitting function of Eq. (57) to fit the exact numerical solution of $\rho_{11}(t)$. The results show that with the decay function $f_h(t) = 0.48\exp(-0.58t) + 0.50$ and $f_l(t) = -0.47\exp(-0.54t) + 0.49$, fitting function (57) gives very much the same solution as that obtained numerically from Eq. (52) for $\rho_{11}(t)$.

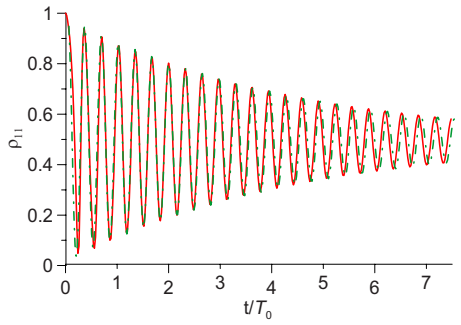

FIG. 17. (Color online) (a) Using the fitting function $f_h(t)\cos^2(\langle\Omega\rangle t/2) + f_l(t)\sin^2(\langle\Omega\rangle t/2)$ (the red solid line) to fit the exact numerical solution of $\rho_{11}(t)$ (the green dashed-dotted line). Here we use the parameters $\mu - E = 50\ \mu$eV, $\Gamma_{L,R} = 25\ \mu$eV, and $d_{L,R} = 25\ \mu$eV.

In order to have a better fitting to various tunable parameters, we plot in Fig. 18 the fitting errors for $\rho_{11}(t)$ by averaging the deviations between $f_h(t)$ and the peaks of the os-

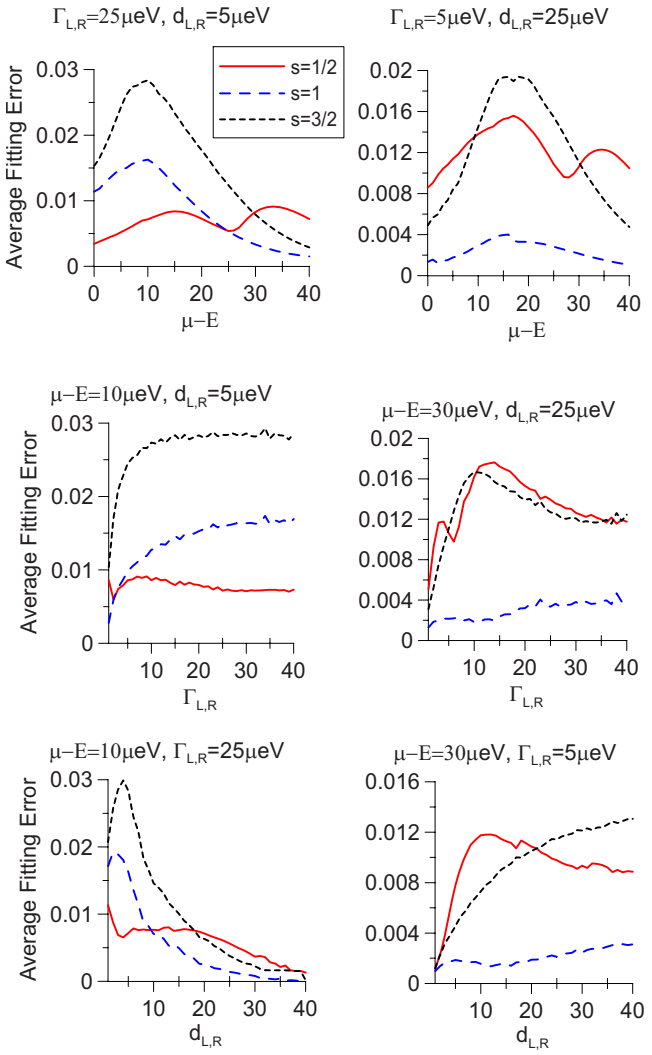

FIG. 18. (Color online) The average fitting errors by fitting the exact numerical solutions of $\rho_{11}(t)$ with the fitting function given by Eq. (57). The top two plots are the fitting errors by varying $\mu-E$ but fixing $(\Gamma_{L,R},d_{L,R})=(25,5)$ μeV and $(5,25)$ μeV, respectively. The middle two plots for varying $\Gamma_{L,R}$ but fixing $(\mu-E,d_{L,R})=(10,5)$ μeV and $(30,25)$ μeV, and the bottom two plots are obtained by varying $d_{L,R}$ but fixed $(\mu-E,\Gamma_{L,R})=(10,25)$ μeV and $(30,5)$ μeV. The parameters are chosen such that the left three figures correspond to the non-Markovian regime while the right three figures are the Markovian limit. $s=1/2$ corresponds to the subexponential fitting (red lines), $s=1$ is the simple exponential fitting (blue long-dashed lines), and $s=3/2$ is the superexponential fitting (black dashed lines).

cillating $\rho_{11}(t)$ in a large range of the chemical potential, the tunneling rate as well as the spectral width. The top two plots in Fig. 18 are the fitting errors by varying $\mu_{L,R}$ but fixing $(\Gamma_{L,R},d_{L,R})=(25,5)$ μeV (the strong non-Markovian regime) and $(5,25)$ μeV (the Markovian limit regime). We find that in the strong non-Markovian regime, when the Fermi surfaces are not far away from the resonant levels of the double dot ($\mu-E<25$ μeV), the best fitting is a subexponential decay with $s<1$. When $\mu-E>25$ μeV, the fitting function becomes a simple exponential decay function ($s=1$), while, in the Markovian limit, the best fitting is just a simple exponential decay for all the values of $\mu-E$. The middle two plots in Fig. 18 are the fitting errors by varying $\Gamma_{L,R}$ but fixing $(\mu-E,d_{L,R})=(10,5)$ μeV (the non-Markovian regime) and $(30,25)$ μeV (the Markovian limit). Again we see that in the non-Markovian regime, the best fitting is a subexponential decay with $s<1$ for all the values of $\Gamma_{L,R}$ except for some very small $\Gamma_{L,R}$ ($<\Delta/2$) which indeed enters the Markovian limit where the fitting function becomes a simple exponential decay function. In the Markovian limit (the large spectral width limit here), the best fitting is given by a simple exponential decay ($s=1$) again. The bottom two plots in Fig. 18 are the fitting errors by varying $d_{L,R}$ but fixed $(\mu-E,\Gamma_{L,R})=(10,25)$ μeV (the non-Markovian regime) and $(30,5)$ μeV (the Markovian limit). It tells that in the non-Markovian regime, when $d_{L,R}<\Delta$ (the strong non-Markovian regime), the best fitting is still given by a subexponential decay ($s<1$), while for $d_{L,R}>\Delta$ the system transits to the Markovian, the fitting function becomes again a simple exponential decay function. In the Markovian limit (small tunneling rate limit), the best fitting is just given by a simple exponential decay ($s=1$), as one expected.

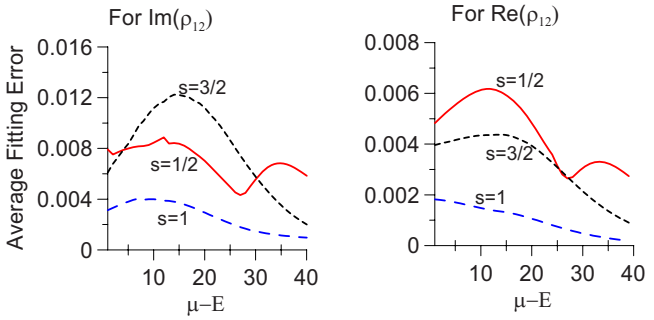

FIG. 19. (Color online) The average fitting errors by fitting the exact numerical solution of Im $\rho_{12}(t)$ and Re $\rho_{12}(t)$ with the fitting functions given by Eq. (58), where we vary $\mu-E$ but fixing $d_{L,R}=5$ μeV and $\Gamma_{L,R}=25$ μeV. The red lines correspond to the subexponential fitting function ($s=1/2$), the blue long-dashed lines are the simple exponential fitting function ($s=1$), and the black dashed lines are the superexponential fitting function ($s=3/2$).

The above analysis shows that Markovian decoherence processes lead to an exponential decay and a subexponential decay seems to occur mainly in strong non-Markovian processes. But this does not imply a simple exponential decay being necessarily Markovian. In Fig. 19, we plot the average fitting errors of fitting function (58) with the exact numerical solution of the real and imaginary parts of the off-diagonal density-matrix element $\rho_{12}(t)$ in the strong non-Markovian regime with the spectral widths $d_{L,R}=5$ μeV and the tunneling rates $\Gamma_{L,R}=25$ μeV. The results show that for both Im $\rho_{12}(t)$ and Re $\rho_{12}(t)$, the best fitting is given by simple exponential decay for the whole range of chemical potential up to $\mu-E=40$ μeV. This forces us to carefully look at the results in Fig. 18. We find that all the results with a subexponential decay show up for small $\mu-E$ values ($<2\Delta$) where the charge leakage effect cannot be effectively suppressed by the chemical potentials of the reservoirs. This tells that the subexponential decay in $\rho_{11}(t)$ is a charge leakage effect. The slightly different decay behaviors for $\rho_{11}(t)$ and Im $\rho_{12}(t)$ actually come from the charge leakage effect contained in

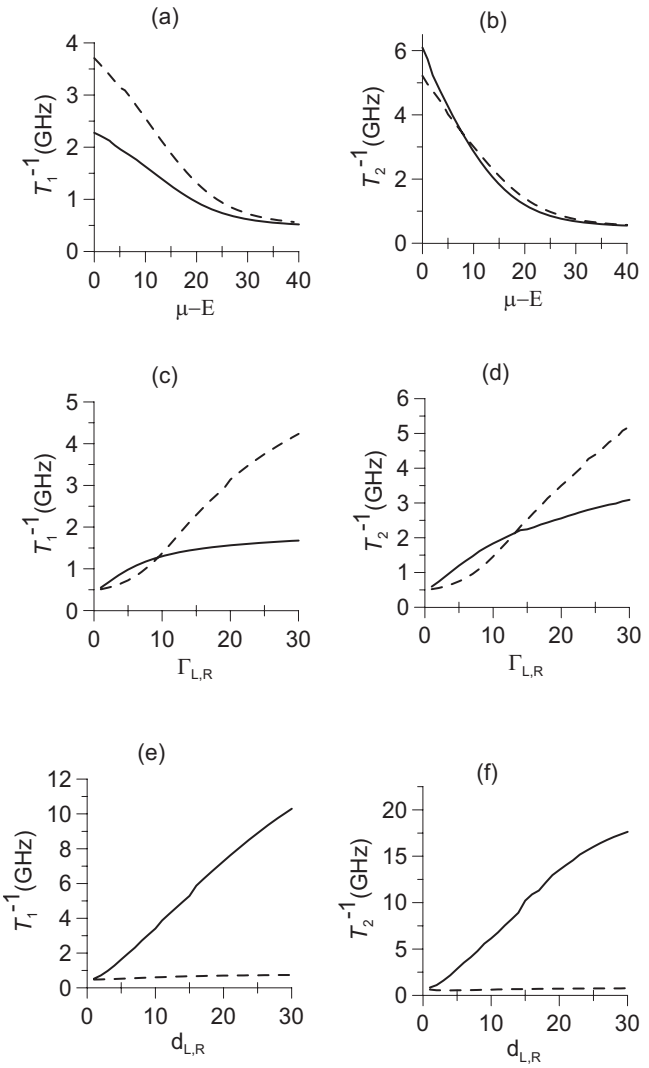

FIG. 20. The relaxation time T_1 and the dephasing time T_2 extracted from Re $\rho_{12}(t)$ and Im $\rho_{12}(t)$, respectively, [(a) and (b)] by varying the chemical potential $\mu-E$ but fixing $(\Gamma_{L,R},d_{L,R})=(25,5)$ (solid lines) and (5,25) μeV (dashed lines), [(c) and (d)] by varying the tunneling rates $\Gamma_{L,R}$ at $(\mu-E,d_{L,R})=(10,5)$ (solid lines) and (30,25) μeV (dashed lines), and [(e) and (f)] by varying the spectral widths $d_{L,R}$ but fixing $(\mu-E,\Gamma_{L,R})=(10,25)$ (solid lines) and (30,5) μeV (dashed lines).

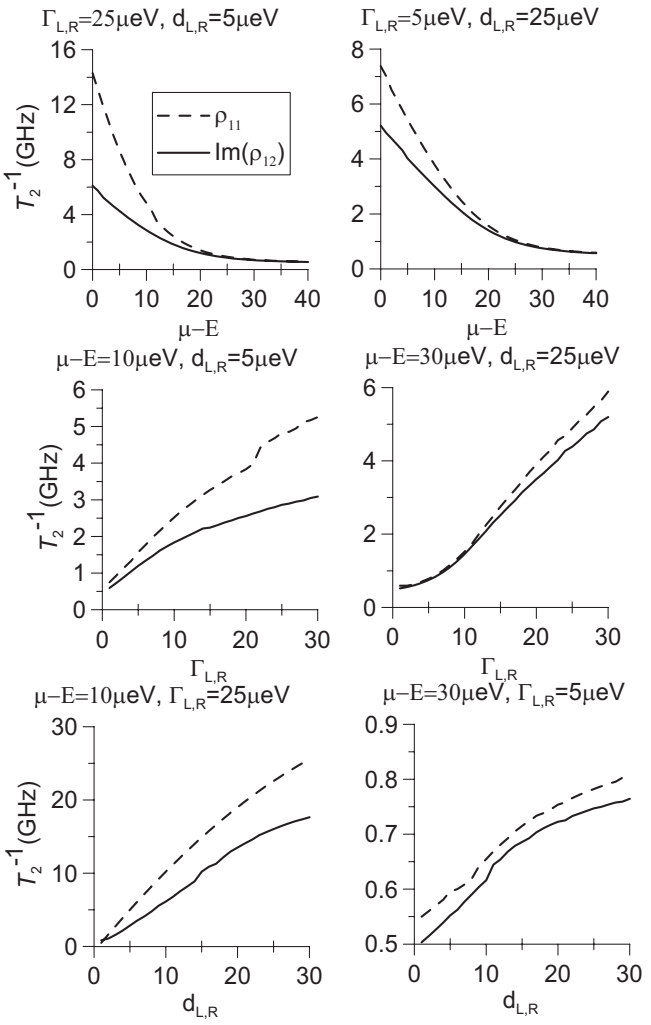

FIG. 21. The decoherence time T_2 extracted from $\rho_{11}(t)$ and Im $\rho_{12}(t)$, respectively, with the same conditions used in Fig. 20, namely, by varying the chemical potential $\mu-E$, the tunneling rates $\Gamma_{L,R}$, and the spectral widths $d_{L,R}$.

$\rho_{11}(t)$ rather than a consequence of non-Markovian dynamics, as we will see more later.

Now we shall extract the relaxation time T_1 from Re $\rho_{12}(t)$ and the decoherence time T_2 from Im $\rho_{12}(t)$ or $\rho_{11}(t)$ using the concept of half-life from the exact numerical solutions and from fitting functions (58) and (57). The results are plotted in Figs. 20–22. In Fig. 20 we plot the relaxation time T_1 and the decoherence time T_2 from Re $\rho_{12}(t)$ and Im $\rho_{12}(t)$, respectively, by varying the chemical potential $\mu-E$, the tunneling rates $\Gamma_{L,R}$, and the spectral widths $d_{L,R}$. Figures 20(a) and 20(b) are the plots of T_1 and T_2 by varying $\mu-E$ but fixing $(\Gamma_{L,R},d_{L,R})=(25,5)$ μeV (solid lines, corresponding to the non-Markovian processes) and (5,25) μeV (dashed lines for Markovian limit). The results tell us that the decoherence effect (for both T_1 and T_2) is large for the small chemical potential $\mu-E$ due to the large charge leakage effect. Increasing $\mu-E$ reduces the charge leakage effect, thus also reducing the decoherence effect. When $\mu-E$ is larger than $\Gamma_{L,R}$ and $d_{L,R}$ [goes up to 30 μeV in Figs. 20(a) and 20(b)], the decoherence effect quickly reaches a minimum value (the longest decoherence time ~2 ns). Figures 20(c) and 20(d) plot T_1 and T_2 by varying $\Gamma_{L,R}$ but fixing $(\mu-E,d_{L,R})=(10,5)$ (solid lines, where both the charge leakage and memory effects are supposed to play an important role) and (30,25) μeV (dashed lines, where both the charge leakage and memory effects are ignorable). It shows that for a small tunneling rate between the reservoir and dot ($<\Delta$) the decoherence effect is weak. Increasing $\Gamma_{L,R}$ enhances the non-Markovian dynamics effect and also enhances the decoherence (shorting the relaxation and dephasing times). Figures 20(e) and 20(f) plot T_1 and T_2 by varying $d_{L,R}$ but fixing $(\mu-E,\Gamma_{L,R})=(10,25)$ (solid lines, where the charge leakage effect dominates) and (30,5) μeV (dashed lines, where the charge leakage effect is negligible). We find that when the memory effect must be considered (corresponding to a small spectral width), the decoherence effect is small (or the relax-

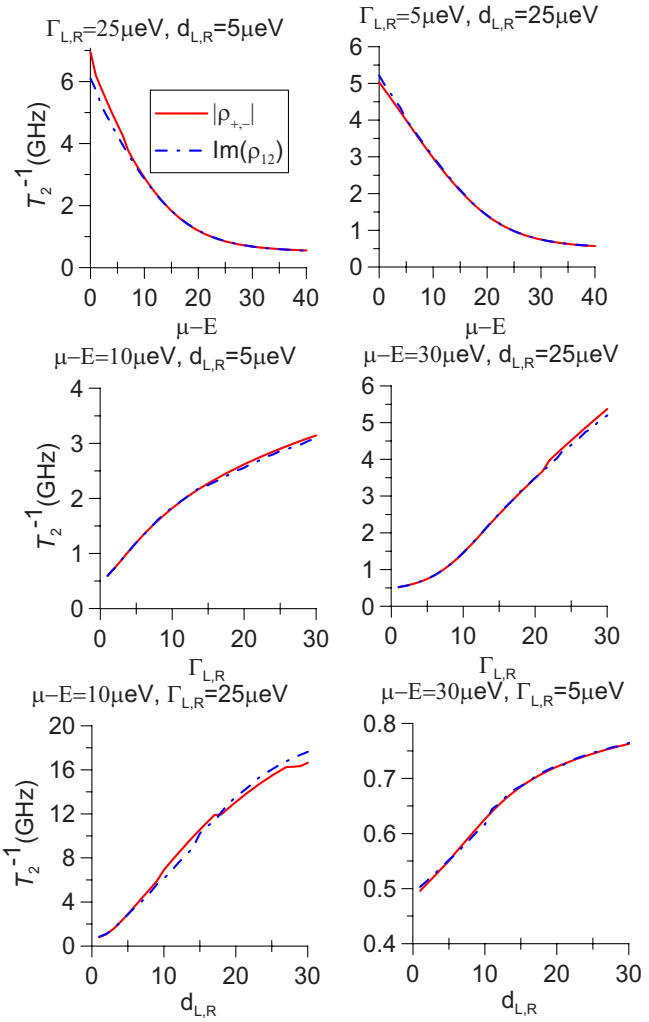

FIG. 22. (Color online) The decoherence time T_2 extracted from $|\rho_{+,-}(t)|=|\langle+|\rho|-\rangle|$ and Im $\rho_{12}(t)$, respectively, with the same conditions used in Fig. 21, namely, by varying the chemical potential $\mu-E$, the tunneling rates $\Gamma_{L,R}$, and the spectral widths $d_{L,R}$.

ation and dephasing times become longer). Increasing $d_{L,R}$ reduces the memory or non-Markovian dynamics effect and enhances the decoherence (shorting the relaxation and dephasing times). It is interesting to see that in all the cases, the relaxation time is close to the dephasing time, $T_1 \simeq T_2$ in the Markovian limit (dashed lines), while for the non-Markovian regime, the relaxation time is no longer than twice the dephasing time, $T_1 \leq 2T_2$ (solid lines).

We have pointed out that the decay behaviors for ρ_{11} and Im ρ_{12} are slightly different from the fitting function in the non-Markovian regime. In Fig. 21, we compare the decoherence time T_2 extracted from $\rho_{11}(t)$ and Im $\rho_{12}(t)$, respectively, with the same conditions used in Fig. 20, namely, by varying the chemical potential $\mu-E$, the tunneling rates $\Gamma_{L,R}$, and the spectral widths $d_{L,R}$. As we see although quantitatively the dephasing times extracted from $\rho_{11}(t)$ and Im $\rho_{12}(t)$ are in the same order, there are some obvious differences in certain range of the tunable parameters where the charge leakage effect plays an important role. This is indeed clearly shown in the right-bottom two plots in Fig. 21 where $\mu-E=30$ μeV. When $\Gamma_{L,R}$ are small ($\leq\Delta/2$) so that the charge leakage is negligible, the dephasing times T_2 extracted from $\rho_{11}(t)$ and Im $\rho_{12}(t)$ are very close to each other over there. This again indicates that it is the charge leakage effect that results in the slightly different decay law for $\rho_{11}(t)$ (follows a subexponential decay) and Im $\rho_{12}(t)$ (by a simple exponential decay) in the non-Markovian regime.

In fact, the original definition of the decoherence for a qubit is given by the decay of $|\langle+|\rho|-\rangle|$ though it is not easy to be measured directly in experiments. Ultimately when the charge qubit is completely decohered, $\rho_{11}\sim\rho_{22}$ and $\mathrm{Im}(\rho_{12})\sim 0$ thus $|\langle+|\rho|-\rangle|\sim 0$ at the asymptotic time. We have verified this property in our exact numerical calculation. Thus the off-diagonal reduced density-matrix element in the energy eigenbasis, $|\langle+|\rho(t)|-\rangle|$, can be well fitted by $Ae^{-Bt^s}+C$, with $C=0$. In Fig. 22 we compare the results of T_2 extracted from $|\langle+|\rho|-\rangle|$ and $\mathrm{Im}(\rho_{12})(t)$. It is remarkable that the dephasing times T_2 obtained from $|\langle+|\rho|-\rangle|$ and $\mathrm{Im}(\rho_{12})(t)$ are almost exactly the same in a wide range of parameters concerned here ($\mu-E$ is from 0 to 40 μeV and $\Gamma_{L,R}$ and $d_{L,R}$ are from 1 to 30 μeV at $\Delta=10$ μeV). The decoherence (dephasing) time T_2 obtained here is between 0.2 and 2 ns, except for the case shown in the left-bottom plot in Fig. 21 where the decoherence time even smaller.

Now we shall end this section with a brief summary in the following. The non-Markovian coherence and decoherence dynamics of charge qubit is dominated by two major effects, the memory and leakage effects in the double dot gated by electrode reservoirs. The former becomes a dominate effect when the time scale of the reservoirs is comparable to the time scale of the double dot. The latter becomes an important effect when the electron tunneling strength between the reservoirs and dots is tuned to be large. These two characters are suitably described by the spectral widths and the tunneling rates embedded in Lorentzian spectral density (25) we used. Strengthening the couplings between the reservoirs and dots and widening the spectral widths of the reservoirs disturb the charge coherence in the double dot significantly. However, reasonably raising up the chemical potentials $\mu_{L,R}$ can suppress charge leakage and maintain charge coherence. The left uncontrollable decoherence factor is the spectral width which characters how many electron states in the reservoirs effectively involving in the tunneling processes between the dots and the reservoirs. The smaller the spectral width is (the less the electron states involve in the electron tunneling), the better the charge coherence can be maintained. The decay of the charge coherent oscillation is well described by a simple exponential decay for the off-diagonal reduced density-matrix elements, but the diagonal ones (populations) are better described by a subexponential law when charge leakage is not negligible. Otherwise simple exponential decay is better for both the non-Markovian and Markovian regimes. The relaxation time T_1 and the dephasing time T_2 can be extracted from the exact numerical solution Re $\rho_{12}(t)$ and Im $\rho_{12}(t)$, respectively, with the result $T_1 \leq 2T_2$ for a broad parameter range we used.

V. FURTHER EXTENSION TO OTHER QUANTUM DOT SYSTEMS

In this section, we shall briefly discuss the possible extension of the present work to other interesting physics in quan-

tum dot systems. The non-Markovian master equation derived in Sec. III can be extended to other quantum dot systems. A prototypical example is a single quantum dot coupled to two electrode leads with spin degrees of freedom of electrons being explicitly taken into account. This system has attracted a lot of interest for the study of Kondo effect, Fano resonance, Coulomb blockade effects, etc.[34–36] The double dots with two electrons for the study of spin entanglement[5] or the double dots through vertical tunnel coupling for the study of two charge qubit entanglement[51] and for the realization of a mesoscopic Aharonov-Bohm interferometer when an external magnetic field is pierced[52–54] are also of great interest. The extended Hamiltonian may generally be written as

$$H = \sum_i E_i a_i^\dagger a_i + \sum_{i\neq j} T_{ij}(a_i^\dagger a_j + a_j^\dagger a_i) + \sum_{ij} U_{ij} n_i n_j + \sum_{\alpha p} \varepsilon_{\alpha p} a_{\alpha p}^\dagger a_{\alpha p} + \sum_{\alpha i p} (t_{i\alpha p} a_i^\dagger a_{\alpha p} + t_{i\alpha p}^* a_{\alpha p}^\dagger a_i), \quad (59)$$

where the index i denotes the electron state in the dot system (including the spin degrees of freedom). The U_{ij} term represents the electron Coulomb repulsion interaction. The index α counts the leads in the reservoir and p labels the electron energy levels as well as electron spins in the reservoir. The last term shows that each level in the dot system may couple to all the external leads.

If the electron Coulomb repulsion term U_{ij} is negligible, the corresponding master equation of the reduced density matrix for the above Hamiltonian still has the same form as Eq. (2) with all the non-Markovian time-dependent coefficient in the master equation being determined by the same relation (34) through the matrices $u(t), v(t)$. Moreover $u(t), v(t)$ still obey the same dissipation-fluctuation equation of motion (30). The only change is the kernel matrices in Eq. (30): $G_{ij}(\tau-\tau')=\Sigma_\alpha F_{ij\alpha}(\tau-\tau')$ and $G_{ij}^\beta(\tau-\tau')=\Sigma_\alpha F_{ij\alpha}^\beta(\tau-\tau')$, where the environmental time correlation functions are now given by

$$F_{ij\alpha}(\tau-\tau') = \sum_p t_{i\alpha p} t_{j\alpha p}^* e^{-i\varepsilon_{\alpha p}(\tau-\tau')}, \quad (60a)$$

$$F_{ij\alpha}^\beta(\tau-\tau') = \sum_p f_\alpha(\varepsilon_{\alpha p}) t_{i\alpha p} t_{j\alpha p}^* e^{-i\varepsilon_{\alpha p}(\tau-\tau')}. \quad (60b)$$

For the case of strong Coulomb repulsion (the Coulomb blockade regime where $U_{ij}\to\infty$), the master equation can describe the electron dynamics in the dots in terms of the Bloch-type rate equations where the double-occupied electron states must be explicitly excluded, as we have discussed in detail in Sec. III D.

When the Coulomb repulsion interaction is comparable to the level energies of electrons in the dots or the external bias, the situation becomes much more complicated. However, studying the above two extreme limits, $U_{ij}\to 0$ and $U_{ij}\to\infty$, together within the same framework could reveal a significant understanding to the quantum transport phenomena, such as Kondo effect.[34] The non-Markovian master equation can also be directly applied to the dynamics of electron entanglement in the doubledot,[5] where we may approximately take the interdot Coulomb repulsion $U_{ij}\to 0$ $(i\neq j)$ and the on-site Coulomb repulsion $U_{ii}\to\infty$. For a finite U_{ij}, existence of a similar rigorous master equation is not obvious and some approximations, such as mean-field approximation or more systematically loop expansion,[55] may be needed. We shall leave these problems for further investigation.

VI. CONCLUSION AND DISCUSSION

In this paper, we have developed a nonperturbation theory to describe decoherence dynamics of electron charges in the double quantum dot gated by electrodes. We extended the Feynman-Vernon influence functional theory to fermionic environments and derived an exact master equation (33) for the reduced density matrix of the double dot without including the interdot Coulomb repulsion at beginning. The contributions of quantum and thermal fluctuations induced by the electron reservoirs are embedded into the time-dependent transport coefficients [Eqs. (34) and (36)] in the master equation. These time-dependent transport coefficients are completely determined by the nonperturbation dissipation-fluctuation equation of motion (30). The exact master equation is then further extended to the double dot in the strong interdot Coulomb interacting regime in terms of Bloch-type rate equation (52) where the strong Coulomb repulsion simply leads one to exclude the states corresponding to a simultaneous occupation of the two dots from Eq. (33). Our theory is developed for a general spectral density of the reservoirs at arbitrary temperatures and bias. Other approximated master equations used for the double quantum dot can be obtained at well-defined limits of the present theory. This nonperturbation decoherence theory allows us to exploit the quantum decoherence dynamics of the charge qubit brought up by the tunneling processes between the reservoirs and dots through qubit manipulations.

We then used the master equation (in terms of the rate equations) to study the non-Markovian decoherence dynamics of the double-dot charge qubit with the backreaction of the reservoirs being fully taken into account. To make qualitative and also quantitative understandings of the charge qubit decoherence, we numerically solve the dissipation-fluctuation integrodifferential equations of motion using a Lorentzian spectral density. We examine the time dependence of all the transport coefficients from which the time scales within which non-Markovian processes become important in the charge coherent dynamics are determined. The correlation time of the electron reservoirs (in terms of the spectral widths in the Lorentzian spectral densities) and the electron tunneling strengths between the reservoirs and dots (in terms of the tunneling rates in the Lorentzian spectral densities) characterize the time scales for the occurrence of non-Markovian processes. Non-Markovian processes dominate the charge coherent dynamics when the spectral width is comparable to the interdot tunnel coupling where the memory effect plays an important role and/or when the tunneling rates between the reservoirs and dots become strong such that charge leakage becomes a main effect for decoherence. Raising up the Fermi surfaces of the reservoirs can suppress charge leakage. The Markovian limit can be

reached with a weak tunneling rate and a large spectral width, where perturbation theory becomes valid and the spectral density is reduced to a constant. The decay of the charge coherent oscillation is well described by a simple exponential law, except for some special regime where the charge leakage is not negligible such that the evolution of state populations is better described by a subexponential decay. We also extracted the relaxation time T_1 and the decoherence time T_2 consistently from different elements of the reduced density matrix and obtained a general result $T_1 \leq 2T_2$ which is on the order of nanoseconds or less in a broad parameter range we considered. These results are ready to be examined in experiments.[1]

Although we concentrate in this paper on the electron charge coherence (decoherence) dynamics in the double quantum dot system, the theory we developed in this work can also be applied to investigate other physical properties, such as quantum transport phenomena and electron entanglement dynamics, in various quantum dot structures. In fact, the spectral density describing the spectral distribution of electron reservoirs and electron tunneling processes between the reservoirs and dots has not been well determined experimentally. We used a Lorentzian spectral density that has been used by others yet is still waiting for justification in experiments. The tunneling rates $\Gamma_{L,R}$ in the Lorentzian spectral density are indeed tunable in experiment and have been extracted from current spectra by assuming a constant spectral density. With the capability of monitoring the time evolution of electronic population transfer, we can look closely at the short-time transport properties in this double-dot device from which we may extract the tunneling rates and the spectral widths for the Lorentzian spectral density or other possible forms of the spectral density. Otherwise it may be other surroundings (phonons and fluctuation in impurity configurations, etc.) that play an important role in the dynamics of charge qubit decoherence. These together with other transport properties in various nanostructures, such as Kondo effect and Fano resonance, as well as electron charge and spin entanglement dynamics in the double dot, deserve a separate study. We will leave these problems to be addressed in separate papers. In short, the theory we developed in this work can be used to study not only the problem of decoherence but also other interesting physics, such as the phenomena of quantum transport as well as the dynamics of electron entanglement in various quantum dot systems.

ACKNOWLEDGMENTS

We would like to thank A. M. van den Brink, S. A. Gurvitz, Y. J. Yan, and X. Q. Li for useful discussions. This work was supported by the National Science Council of ROC under Contract No. NSC-96-2112-M-006-011-MY3.

APPENDIX A: DERIVATION OF THE INFLUENCE FUNCTIONAL

The propagating function governing the time evolution of the reduced density matrix is given by Eq. (22), in which the generalized Feynman-Vernon influence functional is defined by

$$\mathcal{F}[\xi^*,\xi,\eta^*,\eta] = \int d\mu(f_N)d\mu(f_0)d\mu(g_0)\langle f_0|\rho_E(t_0)|g_0\rangle \int \mathcal{D}[f^*,f,g^*,g]e^{i\{S_E[f^*,f]-S_E^*[g^*,g]+S_I[\xi^*,\xi,f^*,f]-S_I^*[\eta^*,\eta,g^*,g]\}}, \tag{A1}$$

where ρ_E is the initial density operator of the fermion reservoirs, f_0, g_0, f_N and their complex conjugates are the Grassmann numbers introduced in the fermion coherent-state representation, S_E is the action of the electron reservoirs, and S_I stands for the action of the interaction between the dots and the reservoirs. Explicitly,

$$\begin{aligned} iS_E[f^*,f] &= \sum_{l=1,2;k} \left\{ \frac{f_{lk}^*(t)f_{lk}(t) + f_{lk}^*(t_0)f_{lk}(t_0)}{2} \right. \\ &\quad \left. + \int_{t_0}^{t} d\tau \left[\left(\frac{\dot{f}_{lk}^* f_{lk} - f_{lk}^* \dot{f}_{lk}}{2} \right) - i\varepsilon_{lk} f_{lk}^* f_{lk} \right] \right\} \\ &= i\sum_{lk} S_{E,lk}[f_{lk}^*, f_{lk}], \end{aligned} \tag{A2a}$$

$$\begin{aligned} S_I[\xi^*,\xi,f^*,f] &= -\sum_{lk} \int_{t_0}^{t} d\tau (t_{ilk}\xi_i^* f_{lk} + t_{ilk}^* f_{lk}^* \xi_i) \\ &= \sum_{lk} S_{I,lk}[\xi_i^*, \xi_i, f_{lk}^*, f_{lk}]. \end{aligned} \tag{A2b}$$

Let the electron reservoirs be initially in a thermal equilibrium state, then

$$\langle f_0|\rho_E(t_0)|g_0\rangle = \prod_{lk} \langle f_{k0}|\frac{1}{Z}e^{-\beta(\varepsilon_{lk}-\mu_l)a_{lk}^\dagger a_{lk}}|g_{k0}\rangle \tag{A3}$$

where $\mu_{L,R}$ are the chemical potentials of the source and drain electron reservoirs connected to dots 1 and 2, respectively, and Z is the fermion partition function of the reservoirs $Z=\Pi_{lk}(e^{-\beta(\varepsilon_{lk}-\mu_l)}+1)$. Obviously, the influence functional can be written as $\mathcal{F}[\xi^*,\xi,\eta^*,\eta]=\Pi_{lk}\mathcal{F}_{lk}[\xi^*,\xi,\eta^*,\eta]$. Furthermore, since the Hamiltonians are quadratic, the path integrals in the influence functional can be exactly calculated using either the Gaussian integrals or the stationary path

method. Here we present the calculation based on the stationary path method. The forward stationary paths of the electrons in the reservoirs are determined by

$$\dot{f}_{lk}(\tau) + i\varepsilon_{lk} f_{lk}(\tau) = -it^*_{ilk}\xi_i(\tau), \tag{A4a}$$

$$\dot{f}^*_{lk}(\tau) - i\varepsilon_{lk} f^*_{lk}(\tau) = it_{ilk}\xi^*_i(\tau), \tag{A4b}$$

with $i=1,2$ for $l=L,R$, respectively. The solutions to stationary path equation (A4) are

$$f_{lk}(\tau) = f_{lk}(t_0)e^{-i\varepsilon_{lk}(\tau-t_0)} - it^*_{ilk}\int_{t_0}^{\tau} d\tau' e^{-i\varepsilon_{lk}(\tau-\tau')}\xi_i(\tau'),$$

$$f^*_{lk}(\tau) = f^*_{lk}(t)e^{i\varepsilon_{lk}(\tau-t)} - it_{ilk}\int_{\tau}^{t} d\tau' e^{i\varepsilon_{lk}(\tau-\tau')}\xi^*_i(\tau'). \tag{A5}$$

With the similar solutions for the backward stationary paths, the lk component of the influence functional is then given by

$$\begin{aligned}\mathcal{F}_{lk}[\xi^*,\xi,\eta^*,\eta] = \exp\Bigg\{ & -|t_{ilk}|^2\int_{t_0}^{t} d\tau \\ & \times\Bigg[\int_{t_0}^{\tau} d\tau' (e^{i\varepsilon_{lk}(\tau-\tau')}\eta^*_i(\tau')\eta_i(\tau) \\ & + e^{-i\varepsilon_{lk}(\tau-\tau')}\xi^*_i(\tau)\xi_i(\tau')) \\ & + \int_{t_0}^{t} d\tau' e^{-i\varepsilon_{lk}(\tau-\tau')}[\eta^*_i(\tau)\xi_i(\tau') \\ & - f(\varepsilon_{lk})[\xi^*_i(\tau)+\eta^*_i(\tau)][\xi_i(\tau')+\eta_i(\tau')]]\Bigg]\Bigg\},\end{aligned} \tag{A6}$$

where $f(\varepsilon_{lk})$ is the Fermi distribution function, $f(\varepsilon_{lk}) = \frac{1}{e^{\beta(\varepsilon_{lk}-\mu_l)}+1}$. Summing up contributions from all fermion modes in the electron reservoirs, we get influence functional (23) with the dissipation-fluctuation kernels given by Eq. (24).

APPENDIX B: DERIVATION OF THE EXACT PROPAGATING FUNCTION

In this appendix we show how to use the solutions of the equations of motion [Eq. (28)] to determine the time-dependent coefficients in the master equation. The equation of motion for $\xi^*_{1,2}$ is just the complex conjugate equation of $\eta_{1,2}$, while that of $\eta^*_{1,2}$ is the complex conjugate to the equation of $\xi_{1,2}$. Meantime both $\xi^*_{1,2}(\tau)$ and $\eta_{1,2}(\tau)$ are fixed at $\tau=t$ and both $\eta^*_{1,2}(\tau)$ and $\xi_{1,2}(\tau)$ are fixed at $\tau=t_0$. We only need to solve the set of equations of motion for $\xi_{1,2}(\tau)$ and $\eta_{1,2}(\tau)$. The solutions to the equations of motion for $\eta^*_{1,2}(\tau)$ and $\xi^*_{1,2}(\tau)$ can be obtained by conjugating the solutions of $\xi_{1,2}(\tau)$ and $\eta_{1,2}(\tau)$ with corresponding replacement of the boundary conditions.

Letting $\chi(\tau)\equiv\xi(\tau)+\eta(\tau)$, equation of motion (28) becomes

$$\begin{aligned}&\dot{\xi}(\tau) + i\begin{pmatrix} E_1 & T_c \\ T_c & E_2\end{pmatrix}\xi(\tau) \\ &\quad + \int_{t_0}^{\tau} d\tau' \begin{pmatrix} F_{1L}(\tau-\tau') & 0 \\ 0 & F_{2R}(\tau-\tau')\end{pmatrix}\xi(\tau') \\ &\quad = \int_{t_0}^{t} d\tau' \begin{pmatrix} F^{\beta}_{1L}(\tau-\tau') & 0 \\ 0 & F^{\beta}_{2R}(\tau-\tau')\end{pmatrix}\chi(\tau'),\end{aligned} \tag{B1a}$$

$$\begin{aligned}&\dot{\chi}(\tau) + i\begin{pmatrix} E_1 & T_c \\ T_c & E_2\end{pmatrix}\chi(\tau) \\ &\quad - \int_{\tau}^{t} d\tau' \begin{pmatrix} F_{1L}(\tau-\tau') & 0 \\ 0 & F_{2R}(\tau-\tau')\end{pmatrix}\chi(\tau') = 0,\end{aligned} \tag{B1b}$$

where we have used the following notations for brevity:

$$\xi(\tau) = \begin{pmatrix}\xi_1(\tau) \\ \xi_2(\tau)\end{pmatrix}, \quad \eta(\tau) = \begin{pmatrix}\eta_1(\tau) \\ \eta_2(\tau)\end{pmatrix}. \tag{B2}$$

To solve the above equations of motion, we introduce the variables $\bar{u}(\tau)$, $u(\tau)$, and $v(\tau)$ such that

$$\chi(\tau) = \bar{u}(\tau)\chi(t), \tag{B3a}$$

$$\xi(\tau) = u(\tau)\xi(t_0) + v(\tau)\chi(t). \tag{B3b}$$

Equation (B1) can then be expressed in terms of the variables $\bar{u}(\tau)$, $u(\tau)$, and $v(\tau)$ as

$$\begin{aligned}&\dot{\bar{u}}(\tau) + i\begin{pmatrix} E_1 & T_c \\ T_c & E_2\end{pmatrix}\bar{u}(\tau) \\ &\quad - \int_{\tau}^{t} d\tau' \begin{pmatrix} F_{1}(\tau-\tau') & 0 \\ 0 & F_{2}(\tau-\tau')\end{pmatrix}\bar{u}(\tau') = 0,\end{aligned} \tag{B4a}$$

$$\begin{aligned}&\dot{u}(\tau) + i\begin{pmatrix} E_1 & T_c \\ T_c & E_2\end{pmatrix}u(\tau) \\ &\quad + \int_{t_0}^{\tau} d\tau' \begin{pmatrix} F_{1L}(\tau-\tau') & 0 \\ 0 & F_{2R}(\tau-\tau')\end{pmatrix}u(\tau') = 0,\end{aligned} \tag{B4b}$$

$$\begin{aligned}&\dot{v}(\tau) + i\begin{pmatrix} E_1 & T_c \\ T_c & E_2\end{pmatrix}v(\tau) \\ &\quad + \int_{t_0}^{\tau} d\tau' \begin{pmatrix} F_{1L}(\tau-\tau') & 0 \\ 0 & F_{2R}(\tau-\tau')\end{pmatrix}v(\tau') \\ &\quad = \int_{t_0}^{t} \begin{pmatrix} F^{\beta}_{1L}(\tau-\tau') & 0 \\ 0 & F^{\beta}_{2R}(\tau-\tau')\end{pmatrix}\bar{u}(\tau'),\end{aligned} \tag{B4c}$$

with the boundary conditions $\bar{u}_{ij}(t)=\delta_{ij}$, $u_{ij}(t_0)=\delta_{ij}$, and $v_{ij}(t_0)=0$, respectively. Obviously, Eq. (B4a) is the backward version of Eq. (B4b). Therefore, $\bar{u}(\tau)=u^{\dagger}(t+t_0-\tau)$ for $t_0 \le \tau \le t$.

Now $\xi_{1,2}(t)$, $\xi^*_{1,2}(t_0)$, $\eta_{1,2}(t_0)$, and $\eta^*_{1,2}(t)$ can be factorized from the boundary conditions, $\xi(t_0)=\xi_0$ and $\eta(t)=\eta_f$. Explicitly, letting $\tau=t_0$ for Eq. (B3a) and $\tau=t$ for Eq. (B3b), we have

$$\xi_0 + \eta(t_0) = \bar{u}(t_0)[\xi(t) + \eta_f], \tag{B5a}$$

$$\xi(t) = u(t)\xi_0 + v(t)[\xi(t) + \eta_f]. \tag{B5b}$$

Note that $\bar{u}(t_0)=u^\dagger(t)$, the above algebraic equation gives solution (29). Similarly, letting $\xi^*(\tau)=[\xi^*_1(\tau)\ \ \xi^*_2(\tau)]$ and $\eta^*(\tau)=[\eta^*_1(\tau)\ \ \eta^*_2(\tau)]$, we have

$$\xi^*(t_0) = \xi^*_f\{I + v^\dagger(t)[I - v^\dagger(t)]^{-1}\}u(t) - \eta^*_0\{I - u^\dagger(t)[I - v^\dagger(t)]^{-1}u(t)\}, \tag{B6a}$$

$$\eta^*(t) = [\eta^*_0 u^\dagger(t) + \xi^*_f v^\dagger(t)][I - v^\dagger(t)]^{-1}. \tag{B6b}$$

Substituting relations (29) and (B6) into propagating function (27) and using the fact that $v(\tau)$ is Hermitian at $\tau=t$, we obtain exact propagating function (31) for the double dot gated by bias electrodes.

*wzhang@mail.ncku.edu.tw

[1] T. Fujisawa, T. Hayashi, and S. Sasaki, Rep. Prog. Phys. **69**, 759 (2006).
[2] R. Hanson, L. P. Kouwenhoven, J. R. Petta, S. Tarucha, and L. M. K. Vandersypen, Rev. Mod. Phys. **79**, 1217 (2007).
[3] J. M. Elzerman, R. Hanson, J. S. Greidanus, L. H. Willems van Beveren, S. De Franceschi, L. M. K. Vandersypen, S. Tarucha, and L. P. Kouwenhoven, Phys. Rev. B **67**, 161308(R) (2003).
[4] T. Hayashi, T. Fujisawa, H. D. Cheong, Y. H. Jeong, and Y. Hirayama, Phys. Rev. Lett. **91**, 226804 (2003); T. Fujisawa, T. Hayashi, H. D. Cheong, Y. H. Jeong, and Y. Hirayama, Physica E (Amsterdam) **21**, 1046 (2004).
[5] J. R. Petta, A. C. Johnson, J. M. Taylor, E. A. Laird, A. Yacoby, M. D. Lukin, C. M. Marcus, M. P. Hanson, and A. C. Gossard, Science **309**, 2180 (2005).
[6] A. K. Hüttel, S. Ludwig, H. Lorenz, K. Eberl, and J. P. Kotthaus, Phys. Rev. B **72**, 081310(R) (2005).
[7] J. Gorman, D. G. Hasko, and D. A. Williams, Phys. Rev. Lett. **95**, 090502 (2005).
[8] R. P. Feynman and F. L. Vernon, Jr., Ann. Phys. **24**, 118 (1963).
[9] S. A. Gurvitz and Ya. S. Prager, Phys. Rev. B **53**, 15932 (1996); S. A. Gurvitz, *ibid.* **57**, 6602 (1998).
[10] T. Fujisawa, T. Hayashi, and Y. Hirayama, J. Vac. Sci. Technol. B **22**, 2035 (2004).
[11] T. Brandes and B. Kramer, Phys. Rev. Lett. **83**, 3021 (1999); T. Brandes and T. Vorrath, Phys. Rev. B **66**, 075341 (2002).
[12] G. M. Palma, K.-A. Suominen, and A. K. Ekert, Proc. R. Soc. London, Ser. A **452**, 567 (1996).
[13] L. Fedichkin and A. Fedorov, Phys. Rev. A **69**, 032311 (2004).
[14] V. N. Stavrou and X. Hu, Phys. Rev. B **72**, 075362 (2005).
[15] C. Karrasch, T. Enss, and V. Meden, Phys. Rev. B **73**, 235337 (2006).
[16] M. Thorwart, J. Eckel, and E. R. Mucciolo, Phys. Rev. B **72**, 235320 (2005).
[17] X. T. Liang, Phys. Rev. B **72**, 245328 (2005).
[18] Z. J. Wu, K. D. Zhu, X. Z. Yuan, Y. W. Jiang, and H. Zheng, Phys. Rev. B **71**, 205323 (2005).
[19] X. Cao and H. Zheng, Phys. Rev. B **76**, 115301 (2007); Phys. Rev. A **75**, 062121 (2007).
[20] S. R. Woodford, A. Bringer, and K. M. Indlekofer, Phys. Rev. B **76**, 064306 (2007).
[21] W. M. Zhang, D. H. Feng, and R. Gilmore, Rev. Mod. Phys. **62**, 867 (1990).
[22] A. J. Leggett, S. Chakravarty, A. T. Dorsey, M. P. A. Fisher, A. Garg, and W. Zwerger, Rev. Mod. Phys. **59**, 1 (1987).
[23] W. H. Zurek, Phys. Rev. D **26**, 1862 (1982).
[24] W. H. Zurek, Phys. Today **44**(10), 36 (1991); Rev. Mod. Phys. **75**, 715 (2003).
[25] A. O. Caldeira and A. J. Leggett, Physica A **121**, 587 (1983).
[26] F. Haake and R. Reibold, Phys. Rev. A **32**, 2462 (1985).
[27] W. G. Unruh and W. H. Zurek, Phys. Rev. D **40**, 1071 (1989).
[28] B. L. Hu, J. P. Paz, and Y. Zhang, Phys. Rev. D **45**, 2843 (1992); Phys. Rev. D **47**, 1576 (1993).
[29] J. H. An and W. M. Zhang, Phys. Rev. A **76**, 042127 (2007).
[30] C. H. Chou, T. Yu, and B. L. Hu, Phys. Rev. E **77**, 011112 (2008).
[31] J. Schwinger, J. Math. Phys. **2**, 407 (1961).
[32] L. V. Keldysh, Sov. Phys. JETP **20**, 1018 (1965).
[33] S. Hershfield, J. H. Davies, and J. W. Wilkins, Phys. Rev. Lett. **67**, 3720 (1991).
[34] Y. Meir, N. S. Wingreen, and P. A. Lee, Phys. Rev. Lett. **70**, 2601 (1993).
[35] J. Konig, J. Schmid, H. Schoeller, and G. Schon, Phys. Rev. B **54**, 16820 (1996); J. Konig, H. Schoeller, and G. Schon, Phys. Rev. Lett. **76**, 1715 (1996).
[36] T. Fujii and K. Ueda, Phys. Rev. B **68**, 155310 (2003).
[37] C. Bruder and H. Schoeller, Phys. Rev. Lett. **72**, 1076 (1994).
[38] J. Lehmann, S. Kohler, P. Hanggi, and A. Nitzan, Phys. Rev. Lett. **88**, 228305 (2002).
[39] J. N. Pedersen and A. Wacker, Phys. Rev. B **72**, 195330 (2005).
[40] X. Q. Li, J. Luo, Y. G. Yang, P. Cui, and Y. J. Yan, Phys. Rev. B **71**, 205304 (2005).
[41] U. Harbola, M. Esposito, and S. Mukamel, Phys. Rev. B **74**, 235309 (2006).
[42] H. Schoeller and G. Schon, Phys. Rev. B **50**, 18436 (1994).
[43] M.-T. Lee and W.-M. Zhang, J. Chem. Phys. **129**, 224106 (2008).
[44] J. Jin, X. Zheng, and Y. J. Yan, J. Chem. Phys. **128**, 234703 (2008).
[45] L. D. Faddeev and A. A. Slavnov, *Gauge Fields: Introduction to Quantum Theory* (Benjamin-Cummings, Reading, MA, 1980).
[46] R. P. Feynman and A. R. Hibbs, *Quantum Mechanics and Path Integrals* (McGraw-Hill, New York, 1965).
[47] H. J. Carmichael, *An Open Systems Approach to Quantum Optics*, Lecture Notes in Physics Vol. m18 (Springer-Verlag, Berlin, 1993).
[48] T. H. Stoof and Yu. V. Nazarov, Phys. Rev. B **53**, 1050 (1996).
[49] B. Elattari and S. A. Gurvitz, Phys. Rev. A **62**, 032102 (2000).

[50] S. Welack, M. Schreiber, and U. Kleinekathoferb, J. Chem. Phys. **124**, 044712 (2006).
[51] S. Weiss, M. Thorwart, and R. Egger, Europhys. Lett. **76**, 905 (2006).
[52] A. W. Holleitner, C. R. Decker, H. Qin, K. Eberl, and R. H. Blick, Phys. Rev. Lett. **87**, 256802 (2001); A. W. Holleitner, R. H. Blick, A. K. Hüttel, K. Eberl, and J. P. Kotthaus, Science **297**, 70 (2002).
[53] J. C. Chen, A. M. Chang, and M. R. Melloch, Phys. Rev. Lett. **92**, 176801 (2004).
[54] M. Sigrist, T. Ihn, K. Ensslin, D. Loss, M. Reinwald, and W. Wegscheider, Phys. Rev. Lett. **96**, 036804 (2006).
[55] W. M. Zhang and L. Wilets, Phys. Rev. C **45**, 1900 (1992).